GRAPHENE-TITANIUM DIOXIDE ELECTRODE CAPACITORS USING MOLECULAR DYNAMICS SIMULATIONS

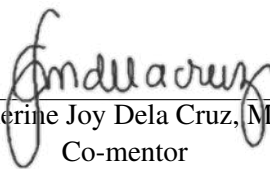**Jesus Emmanuel, II F. Pimentel**

Research report submitted to the Materials Science and Engineering Program, Ateneo de Manila University, School of Science and Engineering in partial fulfillment of the requirements for MATSE 199 and the Bachelor of Science in Materials Science and Engineering degree.

December 2023

Accepted:

_____
Christian Lorenz S. Mahinay, Ph.D.
Mentor

_____
Catherine Joy Dela Cruz, M.S.
Co-mentor

_____
Date

_____
Date

_____
Joel T. Maquiling, Ph.D.
Acting Chair, Physics Department

_____
Jose Mario A. Diaz, Ph.D.
MSE Program Coordinator

_____
Date

_____
Date

Acknowledgements

I would like to thank the following people who have helped me accomplish this study.

First and foremost, to my parents Jay and Sonia, without whom I would not have existed. They gave me the needs of a child, and for that I am very grateful.

To Ms. Dela Cruz, whose insights have proven invaluable to this study. Without you, the idea of this study would not have flourished into this.

To Dr. Mahinay, who provided key insights on a variety of matters throughout the study.

To the Department of Physics and the Materials Science and Engineering group of AdMU, for granting me the opportunity to work on my second degree.

To Migui, Tyler, and Javo, my groupmates since freshman year. Thank you for the gift of friendship. Working with you throughout the years has been nothing short of fun and an honor.

To my labmates: Vera, Chino, Clint, Cath, Liam, David, and the "green card holder" (inside joke) of the group Maya. Never a dull day with you guys around.

ABSTRACT

Due to the ongoing transition to clean energy and the fast progress in mobile technology, electrochemical energy storage (EES) has been a study of interest in society today. This research project aims to simulate EES for supercapacitors using graphene-TiO_2 electrodes and a saline electrolyte using LAMMPS, a classical molecular dynamics simulator. The electrode was generated, minimized, and introduced to a potential drop using LAMMPS. They follow planar and the nano-slit pore models with different pore widths and a constant potential introduced to it. The charge was taken by fitting a best-fit exponential curve into the plot of the charge of form $q(t) = q_{max}(1 - e^{-t/t'})$ where t' is the time at equilibration of the system and q_{max} is the average charge after equilibration. The differential capacitance was found by finding the value of $q(t)$ at $t = 100000$ fs and the potential drop V, using the slope of the best fit line of the plot of Q/V. The calculated quantities and expressions include those of charge and differential capacitance. The results have shown that the nano-slit pore model with $\delta = 3.10$ Å exhibited the highest specific capacitance while the nano-slit pore model with $\delta = 7.10$ Å exhibited the lowest specific capacitance.

"Maybe it's a far stretch
That I won't come undone,
But I would brave the cold edge
To finish up what I've begun."

from "Still Here" by League of Legends, 2WEI, and Forts ft. Tiffany Aris

Table of Contents

List of Tables

List of Figures

<div align="center">

Chapter 1

Introduction

</div>

1.1 Background of the Study

1.1.1 Review of Concepts in Electromagnetism

A capacitor is a device that may be defined as two conductors separated by an insulator along a circuit. These two conductors have equal charges Q, which is the charge stored within the capacitor. The potential drop V of one conductor with respect to the other is proportional to Q. This gives the first definition of capacitance in Equation (1.1), where C represents the capacitance. The SI units for the capacitance is in Farads (F) which is 1 Coulomb per Volt (1 C/V) [1].

$$C = \frac{Q}{V} \tag{1.1}$$

Aside from this definition, it is key to note that the energy itself is stored within the capacitor. Specifically, the energy is found within the electric field in the capacitor, hence its name the electric-field energy. It is best interpreted as electric potential energy. That is, the amount of energy that may be released by the capacitor. This energy U may also be related to the variables in (1.1) by finding the amount of work needed to charge the capacitor. The value of U is shown in (1.2) [1].

$$U = \frac{Q^2}{2C} = \frac{1}{2}QV = \frac{1}{2}CV^2 \tag{1.2}$$

1.1.2 Electrochemical Energy Storage

Electrochemical Energy Storage (EES) is a method of storing electrical energy as chemical energy, essentially a concept of both conversion and storage of energy. The concept dates back to the late 18th century to the early 19th century with Alessandro Volta as the most prominent pioneer with the invention of the Volta pile [2]. They are ubiquitous in today's technology, being used as a method for storing energy for small devices like mobile phones to interactions with the energy grid by combining it with renewable energy sources [3], as well as in different fields such as medicine with pacemakers and hearing aids, automobiles, spacecrafts, and computers

<div align="center">

1

</div>

[2]. The two main methods of electrochemical energy storage is through batteries and through supercapacitors [2].

Classifications of EES systems is done by analyzing three criteria which are their operating temperatures, the electrodes used, and the electrolyte used [2]. In terms of effectiveness, there are three parameters that it must do well in. These are specific power and energy [2], power and energy level and density [4, 5], cycle efficiency, operative characteristics, environmental impact [4], price [2] mainly based on certain costs on recycling, investment and maintenance [4], and shelf life [2, 4].

For electrochemical capacitors, more often known as supercapacitors, the energy is stored either by ion adsorption at the electrode-electrolyte interface for the electric double-layer capacitors or by the redox reactions that happen on electrode surfaces for pseudo-capacitors [4]. Supercapacitors also commonly have longer cycle stability compared to batteries due to less chemical phase changes happening in the electrode during charge-discharge operations. As such, supercapacitors are excellent at charging high amounts of energy and then discharging for high pulse power at short time periods [5]. Designs for these devices will rely heavily on mathematical modelling and simulations to improve [4]. Improvement in this case will be the increased energy storage and power for these supercapacitors.

1.1.3 Molecular Dynamics Simulations

According to [6], for some molecular system and a set of given parameters, Molecular Dynamics (MD) simulations predict how a certain particle or molecule will move over time. While this might be a small scale, MD still has many applications in a variety of fields including but not limited to materials science, biophysics, chemistry, and medicine [7].

MD simulations generally follow Equation 1.3 where the right-hand side is given by Equation 1.4 [7].

$$m_i \ddot{\mathbf{r}}_i = \mathbf{f}_i \tag{1.3}$$

$$\mathbf{f}_i = -\nabla_i V(\mathbf{r}) \tag{1.4}$$

Equation 1.3 related the Newtonian equation of motion for some particle i with the force $\mathbf{f}_i$ whose value is determined by some potential $V(\mathbf{r})$. MD simulations solve these equations for

each particle in a system for each discrete timestep [7]. MD simulations for nonrelativistic systems show changes that follow the Schrödinger equation shown in Equation 1.5.

$$i\hbar\frac{\partial}{\partial t}\Phi\Big(\{\mathbf{r}_i\},\{\mathbf{R}_I\};t\Big) = H\Phi\Big(\{\mathbf{r}_i\},\{\mathbf{R}_I\};t\Big) \tag{1.5}$$

The H on the right-hand side of the equation refers to the Hamiltonian, which is shown in Equation 1.6 [7].

$$H = \sum_I \frac{\hat{P}_I^2}{2M_I} + H_e\Big(\{\mathbf{r}_i\},\{\mathbf{R}_I\}\Big) \tag{1.6}$$

In these cases, the Born-Oppenheimer approximation is assumed (though there are cases where this does not apply), which starts with seeing that the total wave function Φ is a single product of the nuclear and atomic wave functions [7].

1.1.4 Introduction to Relevant Software

The Large Atomic/Molecular Massive Parallel Simulator, abbreviated to LAMMPS, is a method of simulating MD using a classic MD code. Its focus is primarily on materials modelling. It is an open source code with potentials for solid-state materials, soft matter, and course-grained systems. Furthermore, it is generically used as a parallel particle simulator at a variety of scales [8]. This software will be the primary medium for simulating EES in this study.

Visual Molecular Dynamics (VMD) is an open source software typically used to design, visualize, and analyze different molecules. It is typically used for biological systems, though it may be used for other applications due to its capability to interpret Protein Data Bank (PDB) files [9]. These PDB files can come in varieties from deoxyribonucleic acid (DNA) to materials such as graphite. As such, it is possible to generate electrodes using this software and this capability will be used for this study.

The Open Visualization Tool (OVITO) is an open source software for visualizing MD simulations [10]. It allows users to see the evolution of a dynamic system over time with one frame shown for each time step. To do this, it computes the trajectory of each particle in the system in three dimensions and is excellent for predicting particle behavior and, as a consequence, material structures. Simply, data generated from particle-based simulations are visualized using this software [10]. In this study, it will be used as a primary visualization tool for each simulation run.

1.2 Significance of the Study

The applications of EES are widespread for technical fields of study. For example, automobile batteries, laptops, and smartphones all rely on EES to function everyday [2, 11]. Environment-friendly electric vehicles and the aforementioned portable devices require efficient EES systems to function for an acceptable amount of time [12] with significant efforts already being made to increase storage capacity alongside charge-discharge rates with improved safety and longer cycling stability [13]. Furthermore, EES is applied to interact with the energy grid [3] and is targeted to be a possible solution in solving the problem of intermittence for new energy sources [12].

For the case of supercapacitors, there is an increased demand for it since 2013, mainly due to electric vehicles becoming more prominent [5]. Aside from the transportation sector, the fields of electronics, renewable energy and infrastructure, and other electrical applications have shown to take up the market shares of supercapacitors, with grid balancing entering the market in 2020 [5]. In summary, supercapacitors are used in the transport sector for hybrid electric, electric, and fuel cell vehicles, in electronic gadgets that require uninterruptible power supplies, and a supplemental role next to batteries in energy harvesting systems [11]. Such a role in the scientific community and in society cannot be overlooked, and improvements in supercapacitors considering their applications will hopefully benefit the world and help transition to more carbon-neutral and low-emission options. Alongside this, while supercapacitors will likely play a supplemental role in the grid as an energy harvester [11], designing more efficient supercapacitors may also hopefully play a role in the Philippines' program to shift to more renewable energy sources [14].

1.3 Objectives of the Study

This study has three main objectives enumerated in detail below.

1. **Simulate EES for graphene-TiO$_2$ supercapacitors for two different electrode models.** These electrode models are specifically the planar model and the nano-slit pore model. This will be further expounded on in Chapters 2 and 3.

2. **Determine the differential capacitance of each of the electrode models simulated.** The method of determining this will be discussed in Chapter 3.

3. **Determine the electrode model exhibiting the best surface capacitance.** This will also be discussed in Chapter 3.

1.4   Scope and Limitation

The scope of this study is strictly within the realm of MD. The expected values that can be found within this study are Helmholtz capacitance, charge density, and charging time.

Furthermore, only the constant potential model of LAMMPS will be used in this case. Other parameters available are the constrained charge model and the thermo-potentiostat model. Both of these models may be used for further study.

Finally, only the materials for the electrode and the design of the electrode will be the changing variables in this study. The electrodes will only be using either graphene by itself and graphene with a TiO_2 layer separating the graphene from the electrolyte. The electrolyte will be the same as the one used in the example available in LAMMPS.

Chapter 2

Review of Related Literature

2.1 Usage of Graphene-Metal Oxide Materials for Electrodes

Graphene has been a material of interest in the field of EES due to its high surface area of 2630 m^2/g [15, 16], which increases the efficiency of energy and charge storage in EES systems [17], and electric conductivity while also retaining its mechanical properties well [15, 17, 18]. Alongside these properties, addition of a pore or multiple pores of appropriate size allow an increase in the capacitance of the electrode [17] as these pores increase its surface area. The specific capacitance of these graphene electrodes also reach as high as 135 F/g [15, 18]. However, it must be noted that the stacking of graphene during synthesis decreases its surface area compared to the stated value above. Furthermore, its capacitance combined with an aqueous electrolyte is decreased due to its hydrophobic nature that limits the electrolyte's access [16].

On the other hand, transition metal oxides also allow for a high surface area, higher energy density, and chemical stability [19]. Furthermore, they allow fast and reversible faradaic reactions to occur at the electrode-electrolyte interface [18, 19]. Examples of transition metal oxides used for EES applications are RuO_2, Co_3O_4, MnO_2, and ZnO, with RuO_2 considered as an ideal pseudocapacitive electrode material due to its high capacitance and rapid faradaic redox reactions. However, its expensive price due to its lack of natural abundance and its toxicity to the environment make the aforementioned materials more prominent electrodes production [19]. These metal oxides suffer from poor ionic [18] and electric [18, 16, 19] conductivity, which are detrimental to power density and reversible redox cycling performance [18]. Moreover, this decreased conductivity increases the resistance of the supercapacitor [16].

Composites are also becoming prevalent materials to use for electrodes, with graphene-metal oxides being one of the common combinations of materials used for this purpose. In cases of graphene-metal oxide electrodes, the carbon nanostructure allows the transport of charges to be easier and provides physical support leading to a longer cycling life while the metal oxide material increases the capacitance and also allows an increase in energy density that carbon-based materials are not capable of [16].

6

There are two studies involving graphene and titanium dioxide (TiO_2) composites as the materials for electrodes in EES. Both of these studies are experimental in nature and thus do not involve simulations.

The first of these studies involves reduced graphene-oxide (rGO) with analysis of its shape and coupling effects. Figure 2.1 shows the resulting cyclic voltammetry (CV) curves for the hybrid TiO_2 nanobelts (NBs) and nanoparticles (NPs) with different rGO-to-TiO_2 mass ratios at a scanning rate of 2 mV/s [20].

(a)	(b)
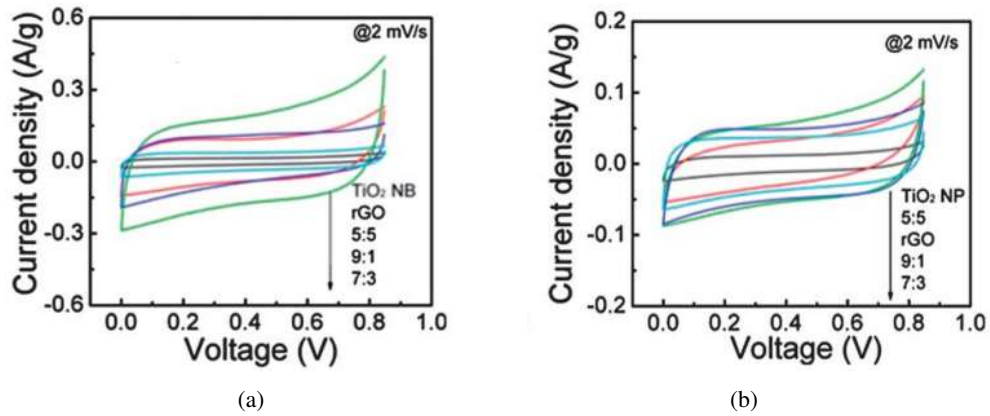
Figure 2.1: The different CV curves for different graphene-TiO_2 ratios at a scanning rate of 2 mV/s for (a) TiO_2 NBs and (b) TiO_2 NPs.

With these curves, it is clear that the integral area of the CV loops for the TiO_2 NBs were much larger than those for the TiO_2 NPs upon inspection of the *y*-axis scales alone. As such, the specific capacitance of the electrodes with TiO_2 NBs is much higher compared to those with the TiO_2 NPs. Furthermore, for both TiO_2 structures, an rGO-to-TiO_2 mass ratio of 7:3 was found to be optimal, exhibiting specific capacitances of 200 F/g and 60 F/g for TiO_2 NBs and TiO_2 NPs, respectively. This higher specific capacitance remains true for different scan rates with measurements of 56.2 F/g and 18.4 F/g for TiO_2 NBs and TiO_2 NPs, respectively [20]. Furthermore, Figure 2.2 shows the charge-discharge behavior of the electrode [20].
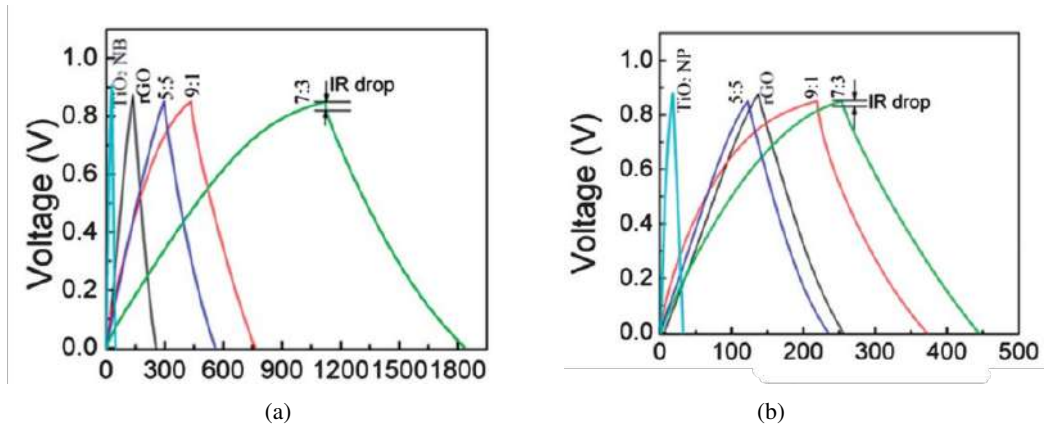
Figure 2.2: The different charge-discharge plots for different graphene-TiO_2 ratios at a current density of 0.125 A/g for (a) TiO_2 NBs and (b) TiO_2 NPs.

From these charge-discharge plots, the specific capacitance for each mass ratio of TiO_2 was calculated. The study paid close attention to the plot of 7:3 graphene-to-TiO_2 mass ratio because it was specified to be the optimal mass ratio. Specific capacitances of 255 F/g and 62.8 F/g were recorded for TiO_2 NBs and TiO_2 NPs, respectively [20]. Moreover, due to its optimal nature, the 7:3 graphene-to-TiO_2 mass ratio was tested in terms of its cycle life where it was found that 86.5% of its original capacitance was retained after 2000 cycles [20]. Finally, the energy and power density was observed. Figure 2.3 shows plots of the power and energy densities for each TiO_2 structure.
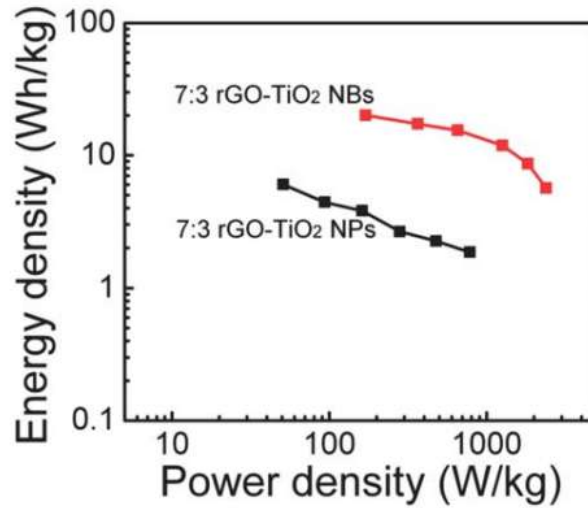
Figure 2.3: Power and energy density plots for TiO_2 NBs and TiO_2 NPs with a 7:3 graphene-to-TiO_2 mass ratio.

From this plot, it is visible that the electrodes with TiO_2 NBs have a higher energy density than those with TiO_2 NPs at the same power density. Furthermore, a higher power density is

8

attainable using TiO_2 NBs instead of TiO_2 NPs [20].

The second study concerns the improvement of activity of a graphene-TiO_2 hybrid capacitor [21]. This differs from the first study in that the first study uses rGO which means that one of the oxygen atoms is still bonded to the graphene whereas this study employs an extra reduction procedure that creates a graphene-TiO_2 composite [21] with no oxide bonds to speak of with the graphene. Furthermore, the electrolyte was identified to be 1M of an Na_2SO_4 solution. As with experimental studies for EES, the three common tests of CV, electrochemical impedance spectroscopy (EIS), and galvanostatic charge-discharge measurements were made [21]. Figure 2.4 shows the CV curves for the graphene-TiO_2 hybrid electrode as well as electrodes with its constituent materials [21].
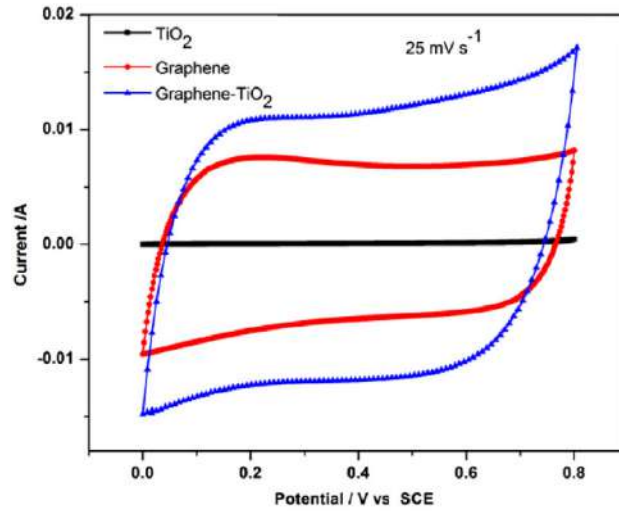
Figure 2.4: The CV curve of the graphene-TiO_2 , graphene, and TiO_2 electrodes at a scanning rate of 25 mV/s.

Based on the areas of the CV loops, it can be seen from Figure 2.4 that the electrode of composite material exhibits the highest specific capacitance. The specific capacitances for the materials are shown in Table 2.1 [21].

Table 2.1: The specific capacitances of electrodes using the different involved materials.

Electrode Material	Specific Capacitance (F/g)
TiO_2	20
Graphene	110
Graphene-TiO_2 hybrid	165

This table shows that the graphene-TiO$_2$ hybrid has the highest specific capacitance among the different materials at the scan rate specified in Figure 2.4. Furthermore, at different scan rates, the CV curves were all approximately rectangular for the hybrid electrodes, which is an indication of good capacitive properties [21]. On the other hand, the EIS yielded Nyquist plots of the aforementioned materials follow a semicircular path for low frequencies and a straight line for high frequencies as shown in Figure 2.5.
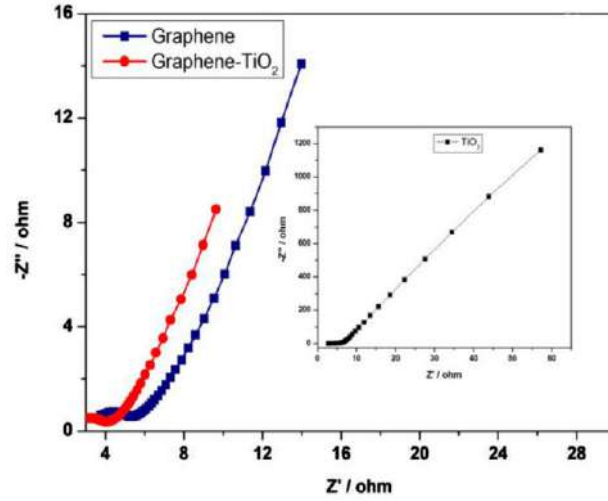
Figure 2.5: Nyquist plots of graphene-TiO$_2$, graphene, and TiO$_2$ (inset graph) with an AC perturbation of 10 mV.

The charge transfer resistance (R_{ct}) is found by taking the semicircular arc in the low-frequency area of the Nyquist plots and measuring its diameter. These yielded the data as shown in Table 2.2 [21].

Table 2.2: The R_{ct} values for each electrode material.

Electrode Material	R_{ct} (Ω)
TiO$_2$	4.1
Graphene	2.0
Graphene-TiO$_2$ hybrid	0.8

Furthermore, Figure 2.5 also allows one to determine the equivalent series resistance (ESR) by determining the intersection between the high-frequency region and the real x-axis of the Nyquist plot. This showed ESR values of 3.0 Ω and 3.5 Ω for the graphene-TiO$_2$ hybrid electrode and the purely graphene electrode, respectively. Having the lowest values for these resistances is also an indication of good capacitive properties [21]. Finally, the galvanostatic

charge-discharge measurements showed curves of triangular shape which is also a good indication of good electrochemical properties. Alongside this, the cycle life of the electrode was also taken, showing only a 9% decrease in specific capacitance after 5000 cycles [21].

These two studies show the viability of the graphene-TiO$_2$ hybrid material in applications of EES. However, it should be duly noted that at the time of writing, the researcher has not yet found a study for simulations with this type of composite material.

2.2 Usage of Molecular Dynamics to Simulate Electrochemical Energy Storage

MD simulations of different kinds have been used to simulate EES. For EES systems based on redox reactions such as in Lithium-ion batteries, *ab initio* MD simulators have been more commonly used due to its implementation of Density Functional Theory (DFT), allowing for an accurate modelling of redox reactions that classical MD simulations cannot provide. This same source also states that the opposite is true for carbon-based electrode materials where redox reactions do not occur [22]. LAMMPS, being a classical molecular dynamics simulator [8], is therefore excellent for simulating EES with carbon-based electrodes. Furthermore, the flexible nature of LAMMPS has allowed some new capabilities to be added to the software [23]. Among these new capabilities is the "ELECTRODE" package [24]. The features of this new package will be discussed at the end of Section 2.2.

Simulations of EES have also already been done in LAMMPS. For example, a comparative study of the capacitance of graphite and graphene-oxide (GO) capacitors with different ionic liquid (IL) electrolytes has been published. It was shown in the study that GO electrodes provide similar or smaller capacitance compared to graphite electrodes and show longer charging relaxation times. Furthermore, the GO electrodes provide a lower energy density. However, it is also worth noting that the graphite electrodes provide a higher cell resistance at voltages greater than or equal to 3.0 V [25].

For graphene-transition metal oxides, one publication served as inspiration for this study. A new electrode design was proposed in this study, which introduced a nano-slit pore of some width δ and compared its findings to an electrode of planar design. Three different δ values were compared in this study which were $\delta = 3.55$ Å, $\delta = 7.10$ Å, and $\delta = 9.23$ Å[26]. These electrode designs are shown in Figure 2.6.
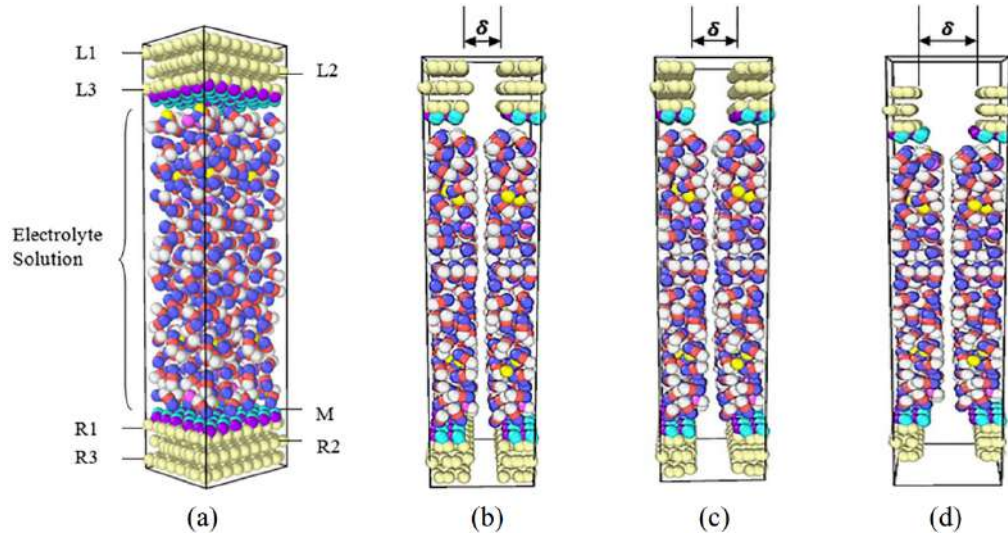
Figure 2.6: Electrode designs following (a) the planar model and the nano-slit pore model with pore widths of (b) $\delta = 3.55$ Å, (c) $\delta = 7.10$ Å, and (d) $\delta = 9.23$ Å.

The dimensions of this simulation domain were defined to be 19.938 Åor 1.9938 nm along the x-axis, 18.520 Åor 1.8520 nm along the y-axis, and 8.040 nm along the z-axis. The distance between the two electrodes was also defined to be 6.105 nm [26]. Figure 2.6 shows these different parts as well, with the graphene electrodes shown in cream, the MnO_2 shown in cyan and violet, and the electrolyte in white, blue, red, and yellow.

The results of this study also show positive results regarding the effect of the addition of both the MnO_2 and the nano-slit pore. Due to the hydrophobic nature of graphene, the usage of an aqueous solution is not ideal because it does not allow the electrolyte access [16], but the addition of the MnO_2 layer increased the capacitance of the electrode with an increased attraction of the solutions ions observed compared to the standalone graphene electrode [26]. With regards to the effect of the slit pore, the Figure 2.7 shows the optimum value of δ to be 7.10 Å due to the finding of maximum partition coefficient. This partition coefficient (Γ) indicates the optimal pore size [26].
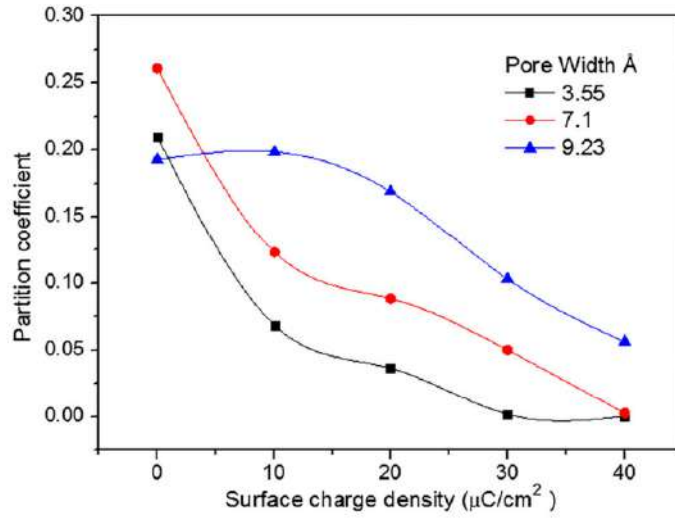
Figure 2.7: Plot of Γ and surface charge density for different δ values.

It can be observed in Figure 2.7 that the highest value of Γ belongs to the pore with $\delta = 7.10$ Å. Using this value of δ, Figure 2.8 shows the plot of the potential in relation to the distance from the graphene surface [26].
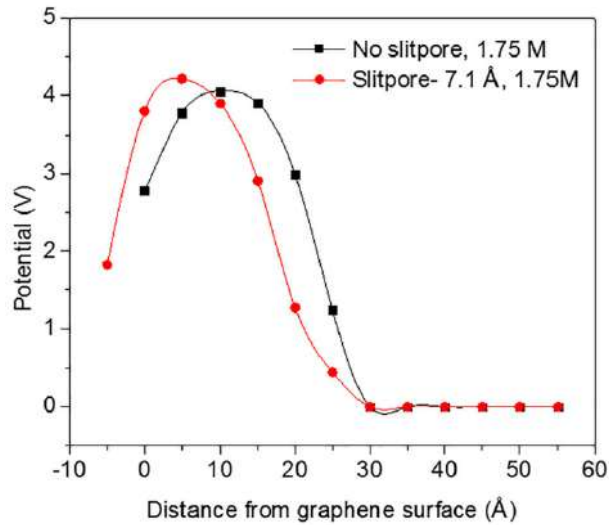
Figure 2.8: Plot of potential and distance from the graphene electrode at $\delta = 7.10$ Å.

It can be observed from Figure 2.8 that the plot of the slit pore model has a higher potential compared to its planar counterpart. With this higher potential and considering that capacitance increases linearly with bias voltage [26, 27], it was therefore concluded that the addition of a nano-slit pore to the electrode with a width of $\delta = 7.10$ Å contributed to an increased capacitance for the graphene-MnO_2 hybrid electrode [26].

At the time of writing this paper, the LAMMPS developers released the most recent version of the software in 2022. This newly released version includes the "ELECTRODE" package whose features will be discussed in this part. The package includes three different charging models to follow which are the constant potential method (CPM), constrained charge method (CCM), and the thermo-potentiostat (TP) [24]. The focus in this part will be the constant potential method.

The usage of CPMs involve modelling conductive electrodes by updating the charges of the individual electrode atoms using the applied electric potential and time-dependent local electrolyte structure [24]. Because it is a classical MD simulator [8], LAMMPS is already excellent at simulating EES without redox reactions such as those with carbon-based electrodes [22]. However, to compensate for the shortcomings on the usage of metals in electrodes, the package also includes "a finite-field approach, multiple corrections for nonperiodic boundary conditions of the particle–particle particle–mesh solver, and a Thomas–Fermi model". The makes LAMMPS a viable option for efficiently simulating EES involving both carbon-based electrodes as well as for electrodes containing unideal metallic materials [24].

Chapter 3

Materials and Methods

3.1 Materials

This study aims to simulate the EES of a graphene-TiO_2 electrode. As such, the reagents used for this study are graphene, TiO_2, water (H_2O), and table salt (NaCl). Due to the simulation nature of this experiment, the purity of the materials is not a concern.

3.2 Methods

3.2.1 Electrode Design

The design of the electrode was done using LAMMPS through the usage of a Windows Subsystem for Linux (WSL). The command lines were ran using Ubuntu 22.04. It involves two main stages, which are the generation and minimization. Both of these stages follow a tutorial found online made by a LAMMPS expert [28]. Without the generation stage, there is no electrode. However, the minimization stage may not be intuitive to most, so its importance will be discussed later in this paper. Furthermore, to separate the electrodes used for this study, a new folder was added to the "electrode" folder called "thesis-me". This was done to avoid confusions with the running of the simulations and to a provide a folder dedicated to this study.

Generation Process

For the generation stage of the electrode design, the code begins by defining units and different styles for the interpretation of atomic data. Alongside this, the specific formulas used to calculate the interactions between atoms are also set.

```
units real
atom_style full
bond_style harmonic
angle_style harmonic
pair_style lj/cut/tip4p/long 1 2 1 1 0.1546 12.0
kspace_style pppm/tip4p 1.0e-4
```

It is likely best to think of this part as a header that includes the different packages needed to run a code.

The lattice of the graphene was then defined in the code, intuitively shown in the "lattice" command. The system was defined as a face-centered cubic (FCC) lattice with a scaling factor of 4.04, that is, the cubic edge length of the lattice is 4.04 Å [29]. The "region" command followed, which defined the region of the "box" within which the atoms will be generated. In essence, the region command "defines a geometric region of space" within which the simulation is run [30]. A "block" style was used to generate a simulation box of dimensions 31 Å × 31 Å × 85.5 Å along the x-, y-, and z-axes, respectively. The "create_box" command then creates a simulation box in which the simulation will occur. The command itself has a number of arguments which are, in order, the number of atom types used in the simulation, number of bond types in the simulation, number of angle types in the simulation, number of bonds per atom, number of angles per atom, and number of special neighbors per atom [31].

```
lattice fcc 4.04
region box block 0 31 0 31 0 85.5 units box
create_box 10 box &

        bond/types 1 &

        angle/types 1 &

        extra/bond/per/atom 2 &

        extra/angle/per/atom 1 &

        extra/special/per/atom 2
```

The graphene parts of the electrode were then defined by simply defining specific spaces where the graphene should be. This consists of three graphene sheets on top of each other, having total thickness of 6.7 Å, with a lattice defined to be hexagonal close-packed with a scaling factor of 2.474 Å. The "create_atoms" command was then used to generate specific atom types within the specified regions [32] based on a file to be discussed later.

```
region rbotwall block 0 31 0 31 0 6.7 units box
region rtopwall block 0 31 0 31 78.8 85.5 units box
lattice hcp 2.474
```

```
create_atoms 5 region rtopwall

create_atoms 8 region rbotwall
```

The creation of the TiO₂ layer then followed. It begins by simply defining the region in which the TiO₂ layers are deposited. The "variable" commands set a specified string or some specified strings as values for something of a given name for use later in the simulation. In this study, the variable command was used to set the lattice structure of the TiO₂ because its values are not set with the correct specifications in LAMMPS, thus requiring manual entry. These variables' values were taken from reference [33].

```
variable a equal 4.60

variable b equal 4.60

variable c equal 2.96

region tio2bot block 0 31 0 31 7.2 11.2 units box

region tio2top block 0 31 0 31 74.8 78.8 units box
```

This was immediately proceeded by the generation of Ti atoms. In these lines of commands, "a1", "a2", and "a3" represent edge vectors of the unit cell under which the Ti atoms are found. On the other hand "basis" defines relative positions, along the a1, a2, and a3 axes. For some command `basis` b_x b_y b_z, some point x is described in terms of the edge vectors as in (3.1) [29].

$$x = b_x \text{a1} + b_y \text{a2} + b_z \text{a3} \tag{3.1}$$

As such, the following command was run for the generation of the Ti atoms. The values for this part were also taken from reference [33].

```
lattice custom 1.0 &

        a1 $a 0.0 0.0 &

        a2 0.0 $b 0.0 &

        a3 0.0 0.0 $c &

        basis 0.5 0.5 0.0

create_atoms 6 region tio2top

create_atoms 9 region tio2bot
```

The same follows for the generation of the O atoms. As with the generation of the Ti atoms, the values for the basis were taken from reference [33]. The following code was used.

```
lattice custom 1.0 &
      a1 $a 0.0 0.0 &
      a2 0.0 $b 0.0 &
      a3 0.0 0.0 $c &
      basis 0.695679 0.695679 0.5
create_atoms 7 region tio2top
create_atoms 10 region tio2bot
```

After this, the generation of the atoms in the electrolyte followed. The electrolyte selected for this study was a solution of H_2O and NaCl. The fluid (H_2O) was generated first, followed by the ion (NaCl) which was generated at random parts [28]. The "molecule" command allows LAMMPS to create atoms based on a template ID [34]. In this case, it was a text file called "TIP4P2005", taken from the tutorial [28]. The "mol" argument under the create_atoms command effectively allows users to create water molecules distributed evenly throughout a three-dimensional space using a template specified using the molecule command [32]. To generate the fluid, the following code was used.

```
region rliquid block 0 31 0 31 11.7 74.3 units box
molecule h2omol TIP4P2005.txt
lattice sc 4.04
create_atoms 0 region rliquid mol h2omol 482793
```

After this, the code to deposit ions into the electrolyte followed. The following lines of code were ran. The "fix" command is used in LAMMPS to apply an operation to a system during timestepping or minimization. The usage of the "deposit" argument allows a user to add new atoms on top of a surface, which in this case is within a defined area [35].

```
fix mydep1 all deposit 10 4 1 56513 region rliquid near 0.3
fix mydep2 all deposit 10 5 1 58613 region rliquid near 0.3
```

Before running the simulation, some specified settings need to be considered by LAMMPS. For example, the first set of numbers seen for each line of code in this part of the study does not mean anything unless they are specified by settings that attach meaning to this number. The following lines of code were ran, with the content of the considered file attached in Appendix A.

```
include ../../PARMtest.lammps
run 10


set type 4 charge 1.0
set type 5 charge -1.0


write_data system.data
write_dump all atom dump.lammpstrj
```

The "run" command runs the simulation for a specified number of timesteps, which themselves correspond to a specific amount of time [36]. On the other hand, the "set" command sets specific properties to the atoms in the system of a specified type [37]. Meanwhile, the "write_data" command enables LAMMPS to write a data file at the end of the simulation [38]. Finally, the "write_dump" command writes user-specified quantities that describe the system [39].

This generated electrode will serve as the planar model for this study. The nano-slit pore model was then created using OVITO. This process involved visualizing the simulation using OVITO and then using a Boolean expression to delete specific atoms from the center of the electrode. In this case, the deletion of atoms happened from the center of the *x*-axis. The expressions used are shown in Appendix B. These files were then exported from OVITO as data files in the "full" atom_style setting to let it remain consistent with the planar model generated.

Minimization Process

It has been mentioned earlier in this paper that there is a necessary minimization process. The process of creating an electrode requires this because the atoms within the electrode are not placed at equilibrium distances from each other. The atoms end up having large amounts of energy between them, causing them to accelerate and the simulation to fail [28].

For the minimization, there were four different sets of code used. These four files only differ depending on the file that they read, which is the data file of each electrode for both the planar and the nano-slit pore model. As with the generation process, the code starts with the definitions of styles and the declaration of the method data is to be interpreted and printed by LAMMPS.

```
boundary p p p
units real
atom_style full
bond_style harmonic
angle_style harmonic
pair_style lj/cut/coul/long 16
kspace_style pppm/electrode 1e-7
```

After this, there are two data files that must be read. First is the data file of the system, found in the first line. The second data file needed is the parameters data file, the one found in Appendix A. This corresponds to two lines, as shown in the code below.

```
read_data ../1gen/system.data
include ../../PARMtest.lammps
```

The next lines of code identify specific types of atoms and lists them under specified groups. Such is the function of the "group" command [40]. The first line declares the group "gH2O" and specifies specific atom types according to the file in Appendix A. On the other hand, the "electrolyte" group is also defined, containing the same atom types as gH2O, but with the addition of the ions. After this, the process dumps a specific set of quantities every 50th timestep using the "dump" command [41].

```
group gH2O type 1 2
group electrolyte type 1 2 3 4
dump mydmp all atom 50 dump.lammpstrj
```

The next commands are all fix commands, actually starting the minimization process. The first fix commands are those with the "nve/limit" and "temp/berendsen" arguments. The first line applies a microcanonical ensemble [42] with a limited step length, which is the maximum limit a molecule or atom can move within the system in one timestep [35, 43]. The next line simply provides a control over the temperature of the system using a Berendsen thermostat, hence the name [35]. After that, the fix command now only affects the electrolyte, with a "shake" argument, which effectively resets the bonds and angles to their equilibrium lengths [44]. On the other hand, the "recenter" argument allows the simulation to constrain the center of mass of a specified group of atoms, which is the electrolyte in this case [35]. The "NULL" and "INIT" arguments specify that for dimensions x, y, and z, the operation is either ignored or set back to its initial value, respectively, [45].

```
fix mynve all nve/limit 0.1
fix myber all temp/berendsen 1 1 1
fix myshk electrolyte shake 1.0e-4 200 0 b 1 a 1
fix myrct electrolyte recenter NULL NULL INIT
```

The following lines are now concerned for running the actual simulation as well as creating the data file of the minimized electrode. The "timestep" command sets the size of the timestep in the simulation [46]. On the other hand, the "thermo" command makes the simulation print out thermodynamic values every specified number of timesteps [47]. The remaining commands left were already discussed in the generation part.

```
timestep 0.5
thermo 50
run 10000
write_data planar_minimized.data
```

3.2.2 Running Simulations

The simulations ran include an equilibration period after the introduction of a potential drop. This is a notable idea to keep in mind considering that this is not seen within the code itself.

As a sample, the code for the planar runs are included. The codes for the other models do not differ much from this. To begin, the first three lines of code are as follows.

```
boundary p p f

include settingsplanar.mod

kspace_modify slab 3.0
```

The first line defines the type of boundary types in this simulation along the x-, y-, and z-axes, respectively [48]. In this case, the simulation box is periodic along the x-, and y-axes, while it is fixed along the z-axis. The "include" command allows LAMMPS to read a settings file that contains specified commands to be discussed later [49]. The third line of the code specifies parameters of the kspace solvers. The "slab" argument allows LAMMPS to use Ewald and PPPM solvers needed for the first line of code [50].

The next lines are as follows.

```
fix conp ebot electrode/conp -1.0 1.979 couple etop 1.0 symm on

dump 1 all custom 50 conp_run.lammpstrj id type xs ys zs vx vy vz
fx fy fz
```

As with the first fix command, the "fix" command applies an operation to the system [35]. In this case, it is applying a constant potential symmetric onto the electrode groups of the simulated box [51]. As mentioned earlier, the "dump" command gives interpreting software a snapshot of the system every specified number of timesteps, which is 50 in this case [41].

The next four lines of code are lines already previously used in the previous section.

```
thermo 50

thermo_style custom step temp c_ctemp1 epair etotal c_qbot c_qtop

write_data conp_planar.data

run 100000
```

The "thermo" command prints thermodynamic properties of the system [47]. The "thermo_style" specifies which values are to be printed out by LAMMPS [52]. Finally, the "run" command runs the simulation for 100000 timesteps.

The settings file plays an important role in the simulation. It specifies the properties of the electrode system and the properties that will be imposed on the simulation itself. The first line of the code is as follows.

```
if "$(extract_setting(world_size) % 2) == 0" then "processors * *
2"
```

This command allows the user to set the default number of processors to work on the simulation to be a multiple of 2.

The next lines of code are definitions, as with the previous section. These lines are presented below, but the explanations are the same as before.

```
atom_style full

pair_style lj/cut/coul/long 16

bond_style harmonic

angle_style harmonic

kspace_style pppm/electrode 1e-7
```

After this, group definitions were defined in the simulation as shown below.

```
group ebot type 8 9 10

group etop type 5 6 7

group water type 1 2

group salt type 3 4

group electrolyte type 1 2 3 4
```

The following lines of code apply different fix operations to the specified groups.

```
fix nvt electrolyte nvt temp 300.0 300.0 100

fix shake water shake 1e-4 20 0 b 1 a 1
```

The first line allows LAMMPS to make time integrations using NVT or the canonical ensembles [35, 53]. The next line [44] applies bond and angle constraints to the electrolyte [44].

The next lines of code command LAMMPS to define a variable and some computations for specific quantities. The "variable" command declares the charge as a variable labelled "q" [54]. On the other hand, the "compute" command lets LAMMPS define computations Specifically, these are the charges on the top and bottom electrodes and the temperature of the electrolyte [55].

```
variable q atom q

compute qtop etop reduce sum v_q

compute qbot ebot reduce sum v_q

compute ctemp1 electrolyte temp
```

For the full codes used, refer to Appendix C.

Aside from this, the behavior of the system's energy was studied briefly for each model at every potential drop value. The potential drop introduced will be varied to four different values: 2.00 V, 1.50 V, 1.00 V, and 0.50 V. The maximum magnitude of the potential drop is set at 2.00 V

3.2.3 Data Analysis

The data analysis was done using Python. The plots of the energy and charge were taken based on the provided values in the log files that LAMMPS creates every time a simulation is run. It is from the charge and the provided potential drop by the user that the capacitance of the electrode is found. This will be explained in better detail later.

The data provided by LAMMPS via the log files includes the temperature and energy of the system and charge of the electrode. For the charge, the data was interpreted as an exponential function of form shown in (3.2) where q represents the charge of an electrode, q_{max} is the maximum charge an electrode can have, t is time, and a, b and k, are real numbers. The value t' is determined numerically as the time point of equilibration, that is, when the energy begins to stabilize. This is taken when the energy reaches its highest point.

$$q(t) = q_{max}(1 - e^{-t/t'}) \qquad (3.2)$$

This is because its slope is practically zero after q_{max} is reached. This concept is crucial because it is expected for any type of EES system that it cannot charge past a certain point. Once it is fully charged, it may not charge further. That said, q_{max} was set to be the average charge of the system after equilibrium.

To find the capacitance, consider the relation between charge Q, potential V, and capacitance C as shown in (3.3).

$$Q = CV \qquad (3.3)$$

The quantity of C is then isolated, leaving what is shown in (3.4). Considering the potential drop V may be defined. In this context, V is the potential difference between the two electrodes. The quantity Q was then taken when $t = 100000$ fs. To do this, Q was modelled after an exponential function using a best fit curve of form as shown in (3.2). With the values of Q and V, we may

incorporate these quantities into (3.4) to arrive at the differential capacitance C_{diff}, given as in (3.5) [56].

$$C = \frac{Q}{V} \tag{3.4}$$

$$C_{\text{diff}} = \frac{dQ}{dV} \tag{3.5}$$

Statistically, this may be interpreted as the slope of the best fit line of the plot Q at $t = 100000$ fs and V [56]. The mass of the system was taken based on the number of atoms of each type in the system, giving the mass of the system in Daltons or amu. This value was then converted to grams. Using these values, the surface capacitance is found, which is defined here as the capacitance per unit area. The conversion factors for the charges from e to Coulombs (C) was defined in reference [57].

Chapter 4

Results and Discussions

4.1 Generated Electrodes

The generation stage of the simulation was successfully ran. The following electrode shown in Figure 4.1.

(a)   (b)   (c)
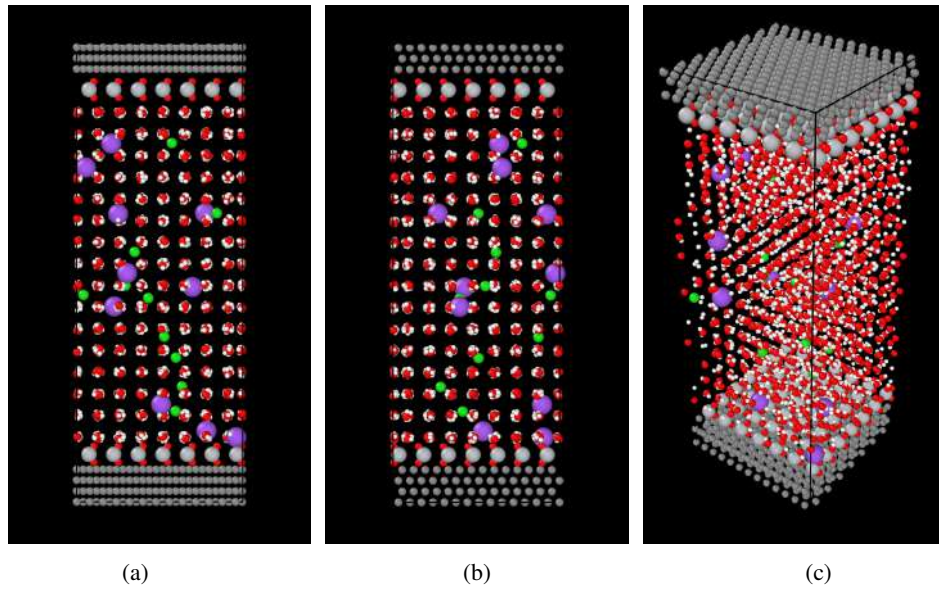
Figure 4.1: Planar electrode resulting from the generation code in the (a) front, (b) left, and (c) perspective views.

This electrode has dimensions of 30.9973 Å × 30.9974 Å × 84.8405 Å. These values were determined using OVITO. It is these values that the software has determined to be optimal and close to the originally assigned values of 31 Å × 31 Å × 85 Å. The rest of the electrodes share these dimensions.

The electrodes that follow the nano-slit pore model were successfully adopted from the planar model using OVITO. Figures 4.2, 4.3, and 4.4.
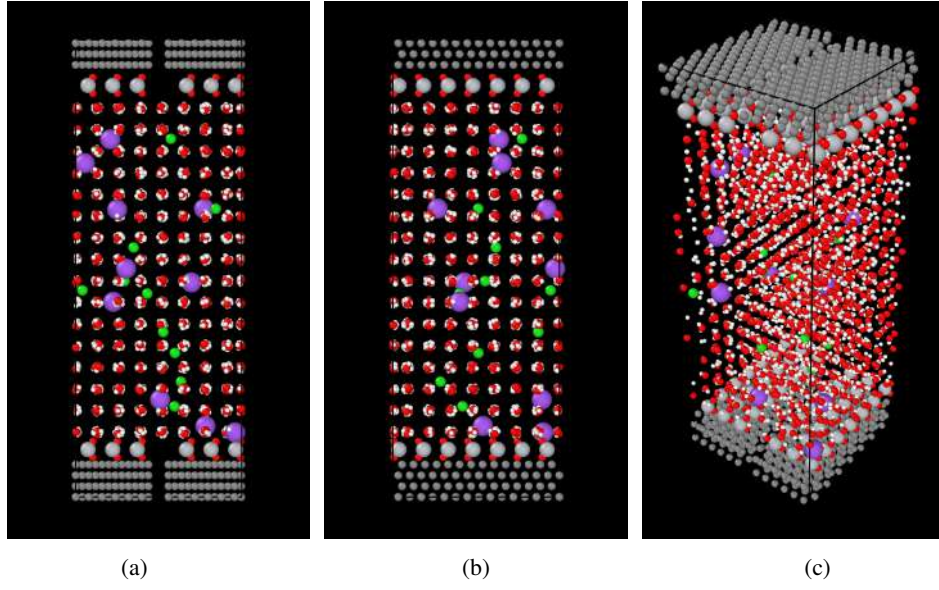
Figure 4.2: Nano-slit pore electrode where $\delta = 3.55$ Å resulting from the generation code in the (a) front, (b) left, and (c) perspective views.
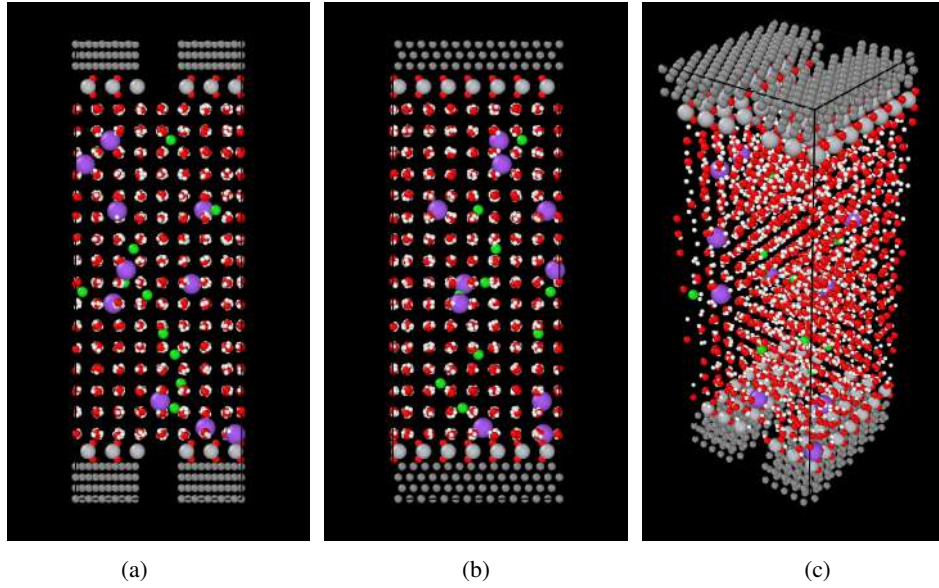
Figure 4.3: Nano-slit pore electrode where $\delta = 7.10$ Å resulting from the generation code in the (a) front, (b) left, and (c) perspective views.
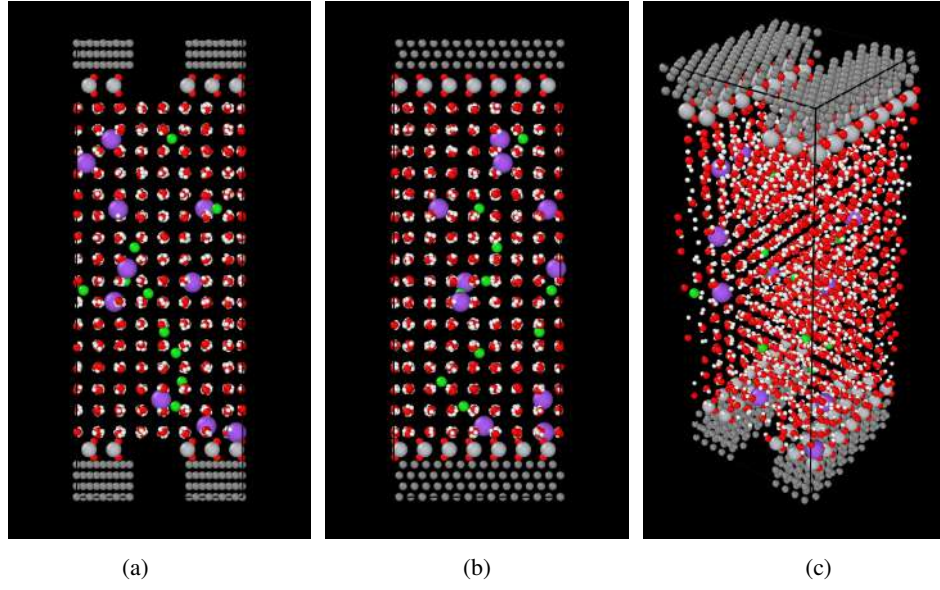
Figure 4.4: Nano-slit pore electrode where $\delta = 9.23$ Å resulting from the generation code in the (a) front, (b) left, and (c) perspective views.

4.2 Minimization of Energy

The energy of the system immediately followed the generation of the electrode samples. A minimization of the energy was exhibited by an amount enough such that the simulation does not fail. Figure 4.5 shows the energy decreases of each of the electrode models.

(a)   (b)

(c)   (d)
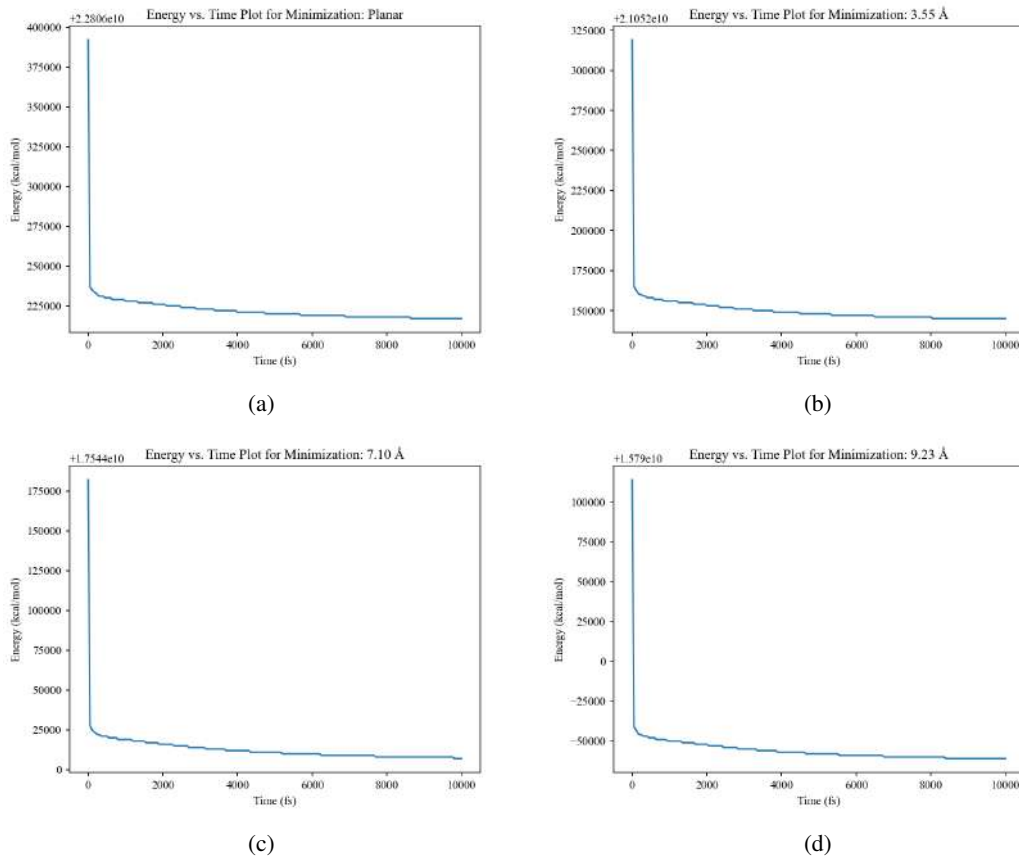
Figure 4.5: Energy plots during the minimization process for the (a) planar model and nano-slit pore models where (b) $\delta = 3.55$ Å, (c) $\delta = 7.10$ Å, and (d) $\delta = 9.23$ Å.

The decrease can be observed with an initial sudden drop, eventually decreasing in small increments. All the values found along the *y*-axis of these plots are additions to the value above the plots. The large drop in energy is of an order of magnitude at 10^4. It is worth noting, however, that the energy minimization in this case was only enough such that the simulation does not fail. In the next section, a spike in the energy of the system is observed, followed by a flattening of the curve around a certain value. This is important to remember for one of the recommendations.

4.3   Energy Data

The energy of the system throughout the simulation after the introduction of a potential drop is discussed in this part. This section is divided into four different subsections, each discussing the behavior of the energy for each value of the potential drop set in the code.

4.3.1   2.0-V Potential Drop

The energy plot for the 2.0-V potential drops are shown in Figure 4.6.

Figure 4.6: Energy plots upon introduction of the potential for the (a) planar model and nano-slit pore models where (b) $\delta = 3.55$ Å, (c) $\delta = 7.10$ Å, and (d) $\delta = 9.23$ Å with a potential drop of 2.0 V.

It can be observed that these plots all have specific maxima before eventually flattening around a certain value. These maxima vary in value, but the timestep at which this maxima is reached is crucial, because that is the value of t' from (3.2). Table 4.1 shows the maximum energies E_{max} reached by the system and the corresponding time t'.

Table 4.1: Maximum energy values and their corresponding timesteps for the electrodes with 2.0 V as introduced potential.

Model	$E_{\max}$ (kcal/mol)	t' (fs)
Planar	42128613	700
Nano-slit pore ($\delta = 3.55$ Å)	39122229	700
Nano-slit pore ($\delta = 7.10$ Å)	33116069	650,700
Nano-slit pore ($\delta = 9.23$ Å)	30111030	700

The t' value for the nano-slit pore with $\delta = 7.10$ Å has two values. For simplicity, the larger value will be taken. As such, the value for t' in its best fit curve will be 700 fs.

4.3.2   1.5-V Potential Drop

The energy plots for each of the models subjected to a 1.5-V potential drop are as shown in Figure 4.7.

(a)

(b)

(c)

(d)

Figure 4.7: Energy plots upon introduction of the potential for the (a) planar model and nano-slit pore models where (b) $\delta = 3.55$ Å, (c) $\delta = 7.10$ Å, and (d) $\delta = 9.23$ Å with a potential drop of 1.5 V.

31

The maximum in each plot is still observed. The t' values for each of these remain consistent as shown in Table 4.2.

Table 4.2: Maximum energy values and their corresponding timesteps for the electrodes with 1.5 V as introduced potential.

Model	E_{max} (kcal/mol)	t' (fs)
Planar	42128604	700
Nano-slit pore ($\delta = 3.55$ Å)	39122266	700
Nano-slit pore ($\delta = 7.10$ Å)	33116098	700
Nano-slit pore ($\delta = 9.23$ Å)	30113051	700

4.3.3   1.0-V Potential Drop

The energy data for the systems where a 1.0 potential drop is introduced are shown in Figure 4.8.
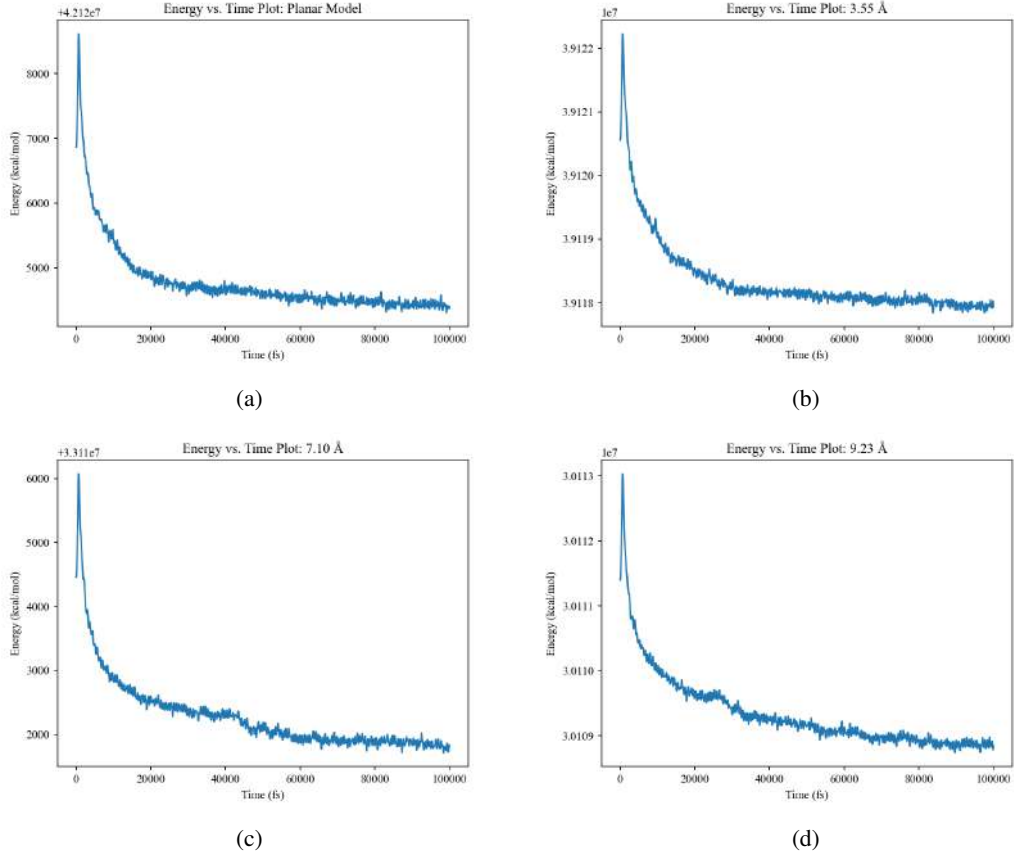

(a)	(b)
(c)	(d)

Figure 4.8: Energy plots upon introduction of the potential for the (a) planar model and nano-slit pore models where (b) $\delta = 3.55$ Å, (c) $\delta = 7.10$ Å, and (d) $\delta = 9.23$ Å with a potential drop of 1.0 V.

As with the other energy plots, there is one maximum that the energy reaches before settling

around an energy value. The t' values are shown to be the same for all the electrodes at 700 fs with differing energy values, as shown in Table 4.3.

Table 4.3: Maximum energy values and their corresponding timesteps for the electrodes with 1.0 V as introduced potential.

Model	$E_{\max}$ (kcal/mol)	t' (fs)
Planar	42128634	700
Nano-slit pore ($\delta = 3.55$ Å)	39122299	700
Nano-slit pore ($\delta = 7.10$ Å)	33116095	700
Nano-slit pore ($\delta = 9.23$ Å)	30113052	700

4.3.4   0.5-V Potential Drop

The energy plots for the electrodes introduced to a 0.5-V potential drop are as shown below for all the electrode models followed.
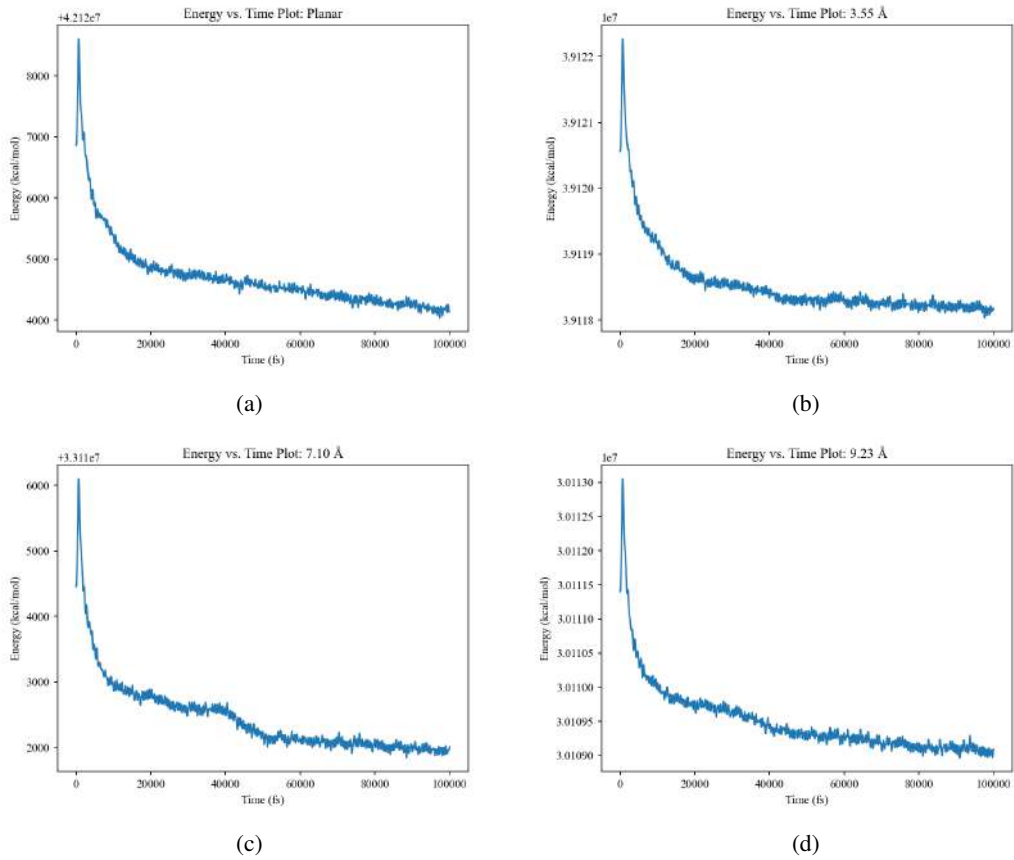

(a)

(b)

(c)

(d)
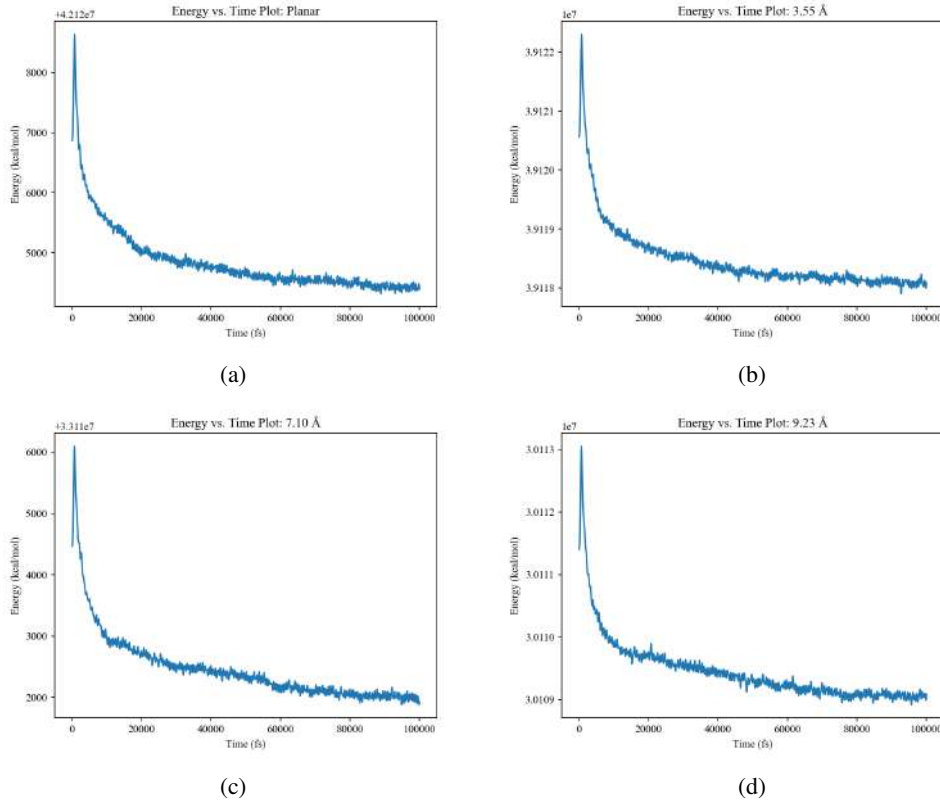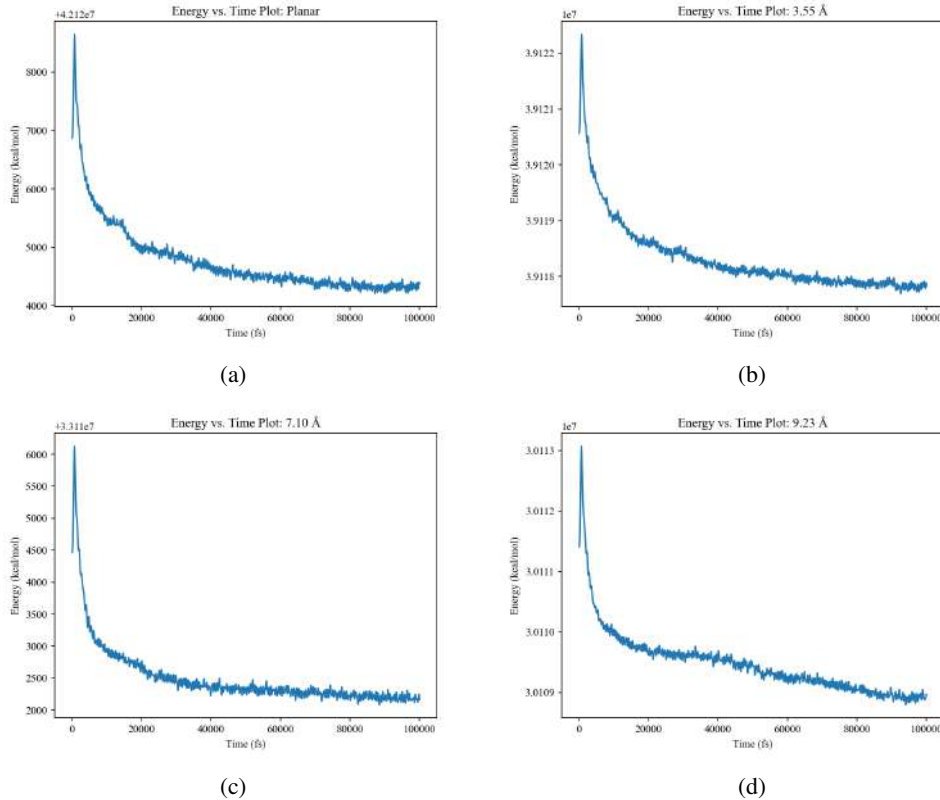
Figure 4.9: Energy plots upon introduction of the potential for the (a) planar model and nano-slit pore models where (b) $\delta = 3.55$ Å, (c) $\delta = 7.10$ Å, and (d) $\delta = 9.23$ Å with a potential drop of 0.5 V.

33

From this, the following values at which the energy reaches its maximum are shown in Table 4.4.

Table 4.4: Maximum energy values and their corresponding timesteps for the electrodes with 0.5 V as introduced potential.

Model	E_{max} (kcal/mol)	t' (fs)
Planar	42128645	700
Nano-slit pore ($\delta = 3.55$ Å)	39122334	750
Nano-slit pore ($\delta = 7.10$ Å)	33116124	700
Nano-slit pore ($\delta = 9.23$ Å)	30113068	700

4.4   Charge Plots

In this section, the charge plots will be shown and discussed for each of the potential drop values, specified by the titles of each subsection. Furthermore, the best fit curves fitted into each of the plots will be discussed.

4.4.1   2.0-V Potential Drop

The average charge at every measurement after time t' is shown for the different models in Table 4.5. This will serve as the values for q_{max}.

Table 4.5: The calculated surface charge q_{max} values at a 2.0-V potential drop.

Model	q_{max} (e/Å)
Planar	0.61464
Nano-slit pore ($\delta = 3.55$ Å)	0.57495
Nano-slit pore ($\delta = 7.10$ Å)	0.40859
Nano-slit pore ($\delta = 9.23$ Å)	0.48549

Figure 4.10 shows the plots of the charges in blue alongside the fitted curve as shown in orange. The different equations for the line of best fit are given beside the orange plot, as well. All the values of $q(100000)$ for each dV is described by q_{max}. As such, these are also the values shown in Table 4.5.

Figure 4.10: Energy plots upon introduction of the potential for the (a) planar model and nano-slit pore models where (b) $\delta = 3.55$ Å, (c) $\delta = 7.10$ Å, and (d) $\delta = 9.23$ Å at a potential drop of 2.0 V.

4.4.2   1.5-V Potential Drop

The average charge values for each of the electrode systems after the measurement at time t' are as follows in Table 4.6.

Table 4.6: The calculated surface charge q_{max} values at a 1.5-V potential drop.

Model	q_{max} (e/Å)
Planar	0.40682
Nano-slit pore ($\delta = 3.55$ Å)	0.47622
Nano-slit pore ($\delta = 7.10$ Å)	0.31587
Nano-slit pore ($\delta = 9.23$ Å)	0.37247

As before, these values were then used for the plots in Figure 4.11, where the blue plot represents the actual behavior of the system and the orange plot shows the fitted curve for the plot after equilibrium.

35

Figure 4.11: Energy plots upon introduction of the potential for the (a) planar model and nano-slit pore models where (b) $\delta = 3.55$ Å, (c) $\delta = 7.10$ Å, and (d) $\delta = 9.23$ Å at a potential drop of 1.5 V.

4.4.3 1.0-V Potential Drop

The average charge at every measurement after time t' is shown for the different models in Table 4.7. As with the previous two processes, this will serve as the values used for q_{max}.

Table 4.7: The calculated surface charge q_{max} values at a 1.0-V potential drop.

Model	q_{max} (e/Å)
Planar	0.35104
Nano-slit pore ($\delta = 3.55$ Å)	0.26569
Nano-slit pore ($\delta = 7.10$ Å)	0.18539
Nano-slit pore ($\delta = 9.23$ Å)	0.16263

This said, the plots shown in Figure 4.12 show the behavior of the charges under 1.0 V of potential drop. The blue plot shows the actual behavior and the orange plot shows the fitted line for the electrode after equilibration.
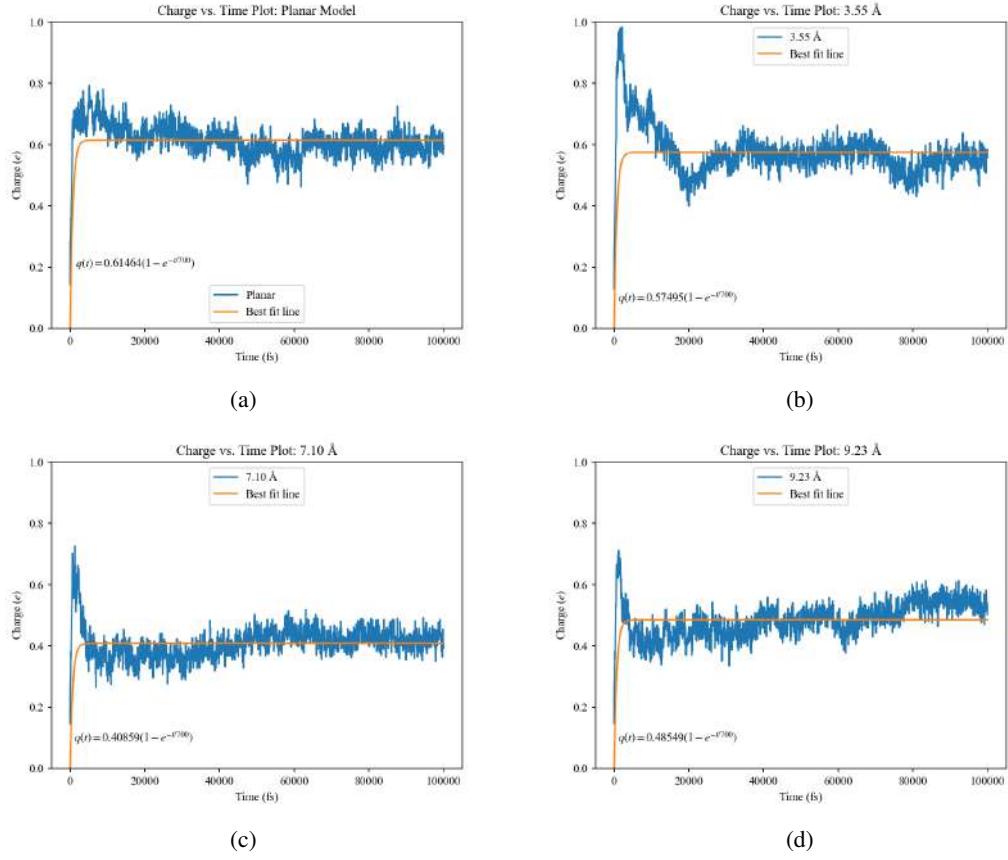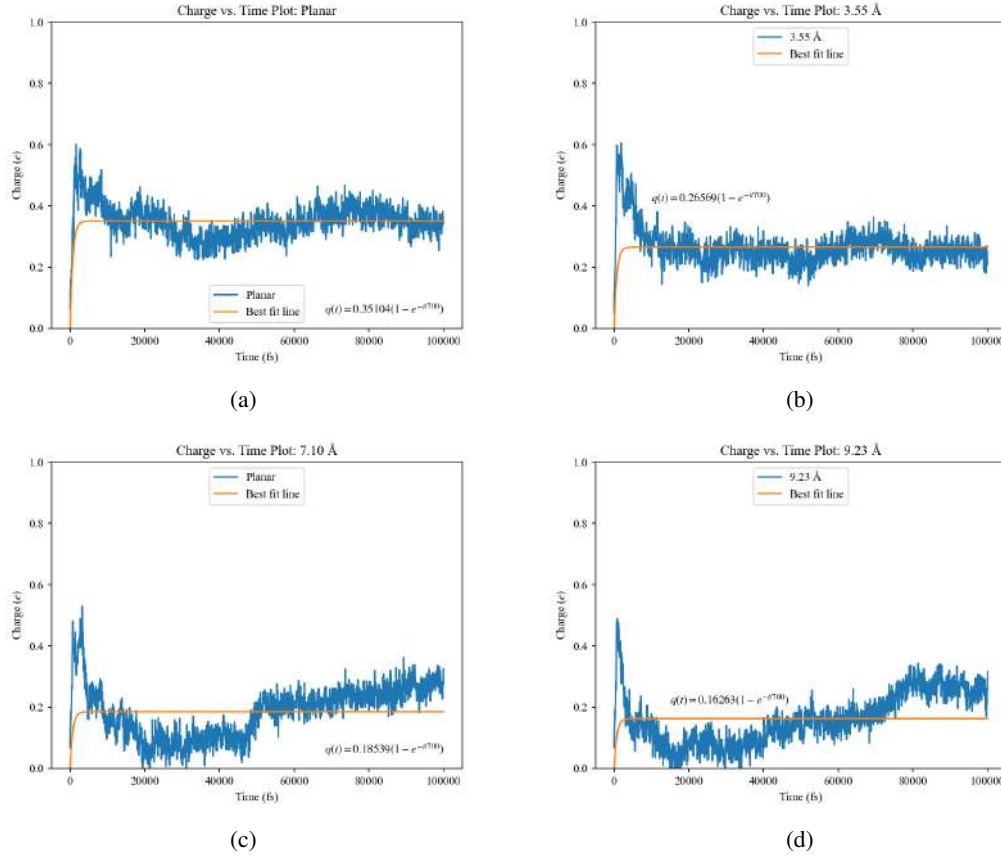
Figure 4.12: Energy plots upon introduction of the potential for the (a) planar model and nano-slit pore models where (b) $\delta = 3.55$ Å, (c) $\delta = 7.10$ Å, and (d) $\delta = 9.23$ Å at a potential drop of 1.0 V.

4.4.4   0.5-V Potential Drop

The average charge value for each model after equilibration is shown in Table 4.8.

Table 4.8: The calculated surface charge q_{max} values at a 0.5-V potential drop.

Model	q_{max} $(e/\text{Å})$
Planar	0.29105
Nano-slit pore ($\delta = 3.55$ Å)	0.18753
Nano-slit pore ($\delta = 7.10$ Å)	0.15448
Nano-slit pore ($\delta = 9.23$ Å)	0.13259

These are then plugged into (3.2). Figure 4.13 shows the different plots of the charges for each electrode. The blue plot shows the actual behavior of the charges of the electrode, while the orange plot shows the fitted curve.
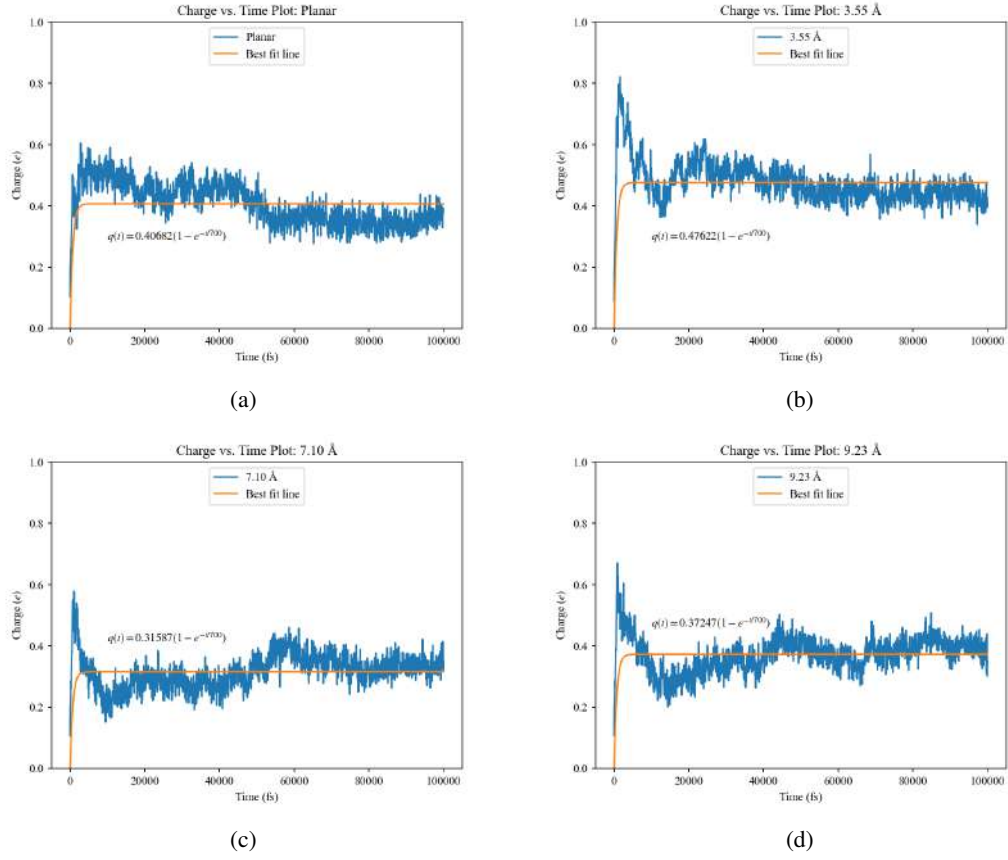
37
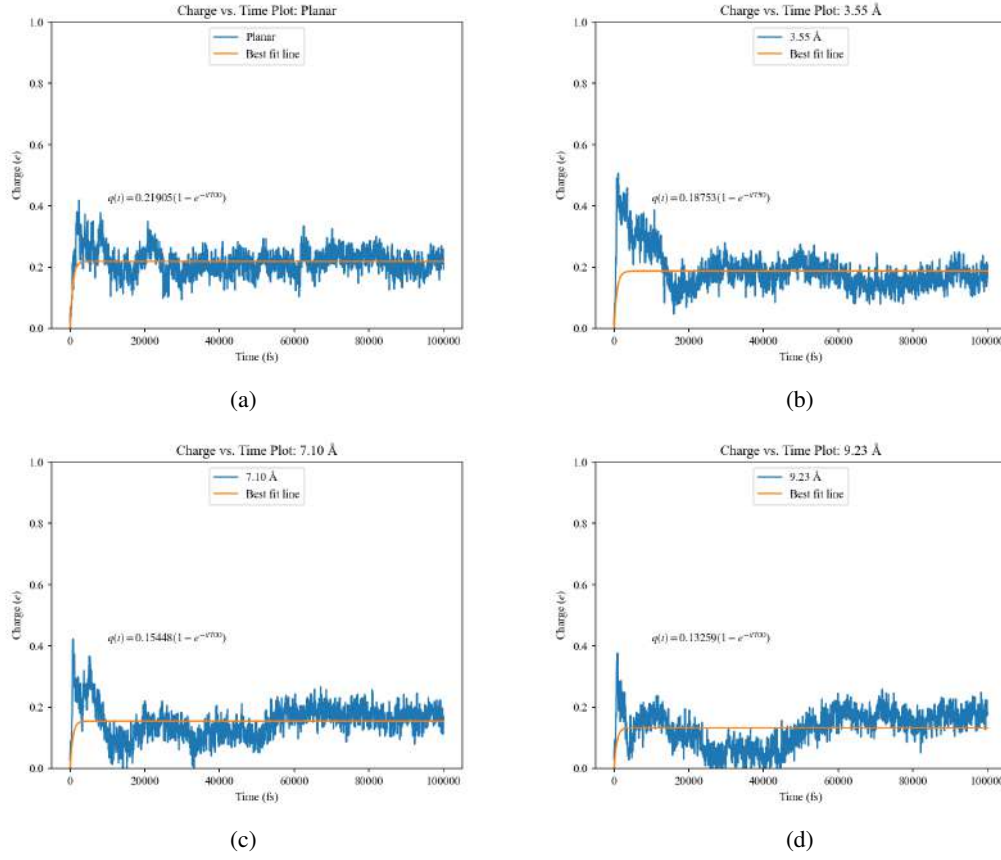
Figure 4.13: Energy plots upon introduction of the potential for the (a) planar model and nano-slit pore models where (b) δ = 3.55 Å, (c) δ = 7.10 Å, and (d) δ = 9.23 Å at a potential drop of 0.5 V.

4.5   Capacitance

The differential capacitance was taken for each of the electrode models by taking the slope of the best fit line of the charge versus potential drop scatter plots.

The scatter plots of the charge at t = 100000 fs against the potential drop on the capacitor is shown in Figure 4.14. These are also accompanied by the best-fit lines of the plots.
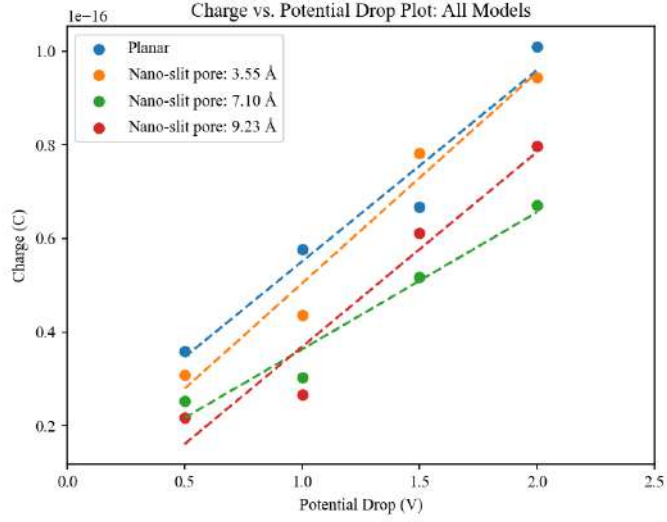
Figure 4.14: Scatter plot and best fit lines of the charge at $t = 100000$ fs vs. potential drop across the capacitor.

Equations (4.1) to (4.4) show the different equations of the best fit line, which we will label arbitrarily as y.

$$y_{\text{planar}} = (4.0880 \times 10^{-17})V + 1.4200 \times 10^{-17} \qquad (4.1)$$

$$y_{3.55\,\text{Å}} = (4.5032 \times 10^{-17})V + 5.3962 \times 10^{-18} \qquad (4.2)$$

$$y_{7.10\,\text{Å}} = (2.9287 \times 10^{-17})V + 7.0330 \times 10^{-18} \qquad (4.3)$$

$$y_{9.23\,\text{Å}} = (4.1613 \times 10^{-17})V - 4.7302 \times 10^{-18} \qquad (4.4)$$

As such, the slope of each of these lines are of degree 10^{-17}. The following values in Table 4.9 are the differential capacitance of each of the capacitors for a specific electrode model.

Table 4.9: Capacitance values taken from equations (4.1) to (4.4).

Model	C_{diff} ($\times 10^{-17}$ F)
Planar	4.0880
Nano-slit pore ($\delta = 3.55$ Å)	4.5032
Nano-slit pore ($\delta = 7.10$ Å)	2.9287
Nano-slit pore ($\delta = 9.23$ Å)	4.1613

The next table shows the surface capacitance measurements for each of the capacitors with different electrode models. Note that these were all taken using the area of the simulation

39

box in the x-y plane. The area therefore comes out to be 960.836 Å^2 or 9.60836×10^{-14} cm^2. From here, the surface capacitance may be calculated. The results are shown in Table 4.10.

Table 4.10: Surface capacitance values for each electrode model.

Model	Surface Capacitance (μF/cm^2)
Planar	425.46
Nano-slit pore ($\delta = 3.55$ Å)	468.68
Nano-slit pore ($\delta = 7.10$ Å)	304.81
Nano-slit pore ($\delta = 9.23$ Å)	433.09

As shown in Table 4.10, the nano-slit pore model with $\delta = 3.10$ Å exhibited the highest surface capacitance value, while the nano-slit pore model with $\delta = 7.10$ Å exhibit the lowest value for surface capacitance. It is important to note that these values are significantly larger than those found in other simulation studies [56]. These inaccuracies are likely due to the fact that the simulating EES itself using a classical dynamics simulator is relatively in its infancy, especially in LAMMPS, where the ELECTRODE package was published only in 2022 [24].

4.6   Electrical Energy Stored

To find the electrical energy stored within the capacitor U, Equation (1.2) in terms of the charge Q and the capacitance C was used. Table 4.11 shows the energy stored by the capacitor at a potential drop of 2.00 V.

Table 4.11: Calculated energy stored by the capacitor at $V = 2.00$ V.

Model	U ($\times 10^{-17}$ J)
Planar	10.95
Nano-slit pore ($\delta = 3.55$ Å)	8.696
Nano-slit pore ($\delta = 7.10$ Å)	6.753
Nano-slit pore ($\delta = 9.23$ Å)	6.710

On the other hand, the values of U at a potential drop of 1.50 V is shown in Table 4.12.

Table 4.12: Calculated energy stored by the capacitor at $V = 1.50$ V.

Model	U ($\times 10^{-17}$ J)
Planar	4.796
Nano-slit pore ($\delta = 3.55$ Å)	5.966
Nano-slit pore ($\delta = 7.10$ Å)	4.036
Nano-slit pore ($\delta = 9.23$ Å)	3.950

Meanwhile, the energy stored by each capacitor at 1.00 V is shown in Table 4.13.

Table 4.13: Calculated energy stored by the capacitor at $V = 1.00$ V.

Model	U ($\times 10^{-17}$ J)
Planar	3.571
Nano-slit pore ($\delta = 3.55$ Å)	1.857
Nano-slit pore ($\delta = 7.10$ Å)	1.390
Nano-slit pore ($\delta = 9.23$ Å)	0.7530

Finally, the values of U at a 0.50-V potential drop are shown in Table 4.14.

Table 4.14: Calculated energy stored by the capacitor at $V = 0.50$ V.

Model	U ($\times 10^{-17}$ J)
Planar	2.455
Nano-slit pore ($\delta = 3.55$ Å)	0.9252
Nano-slit pore ($\delta = 7.10$ Å)	0.9653
Nano-slit pore ($\delta = 9.23$ Å)	0.5005

From these tables, the graphs shown in Figure 4.15 show how the different. These graphs are shown to visualize the differences between the electrical energy stored across the different models at specific potential drops.
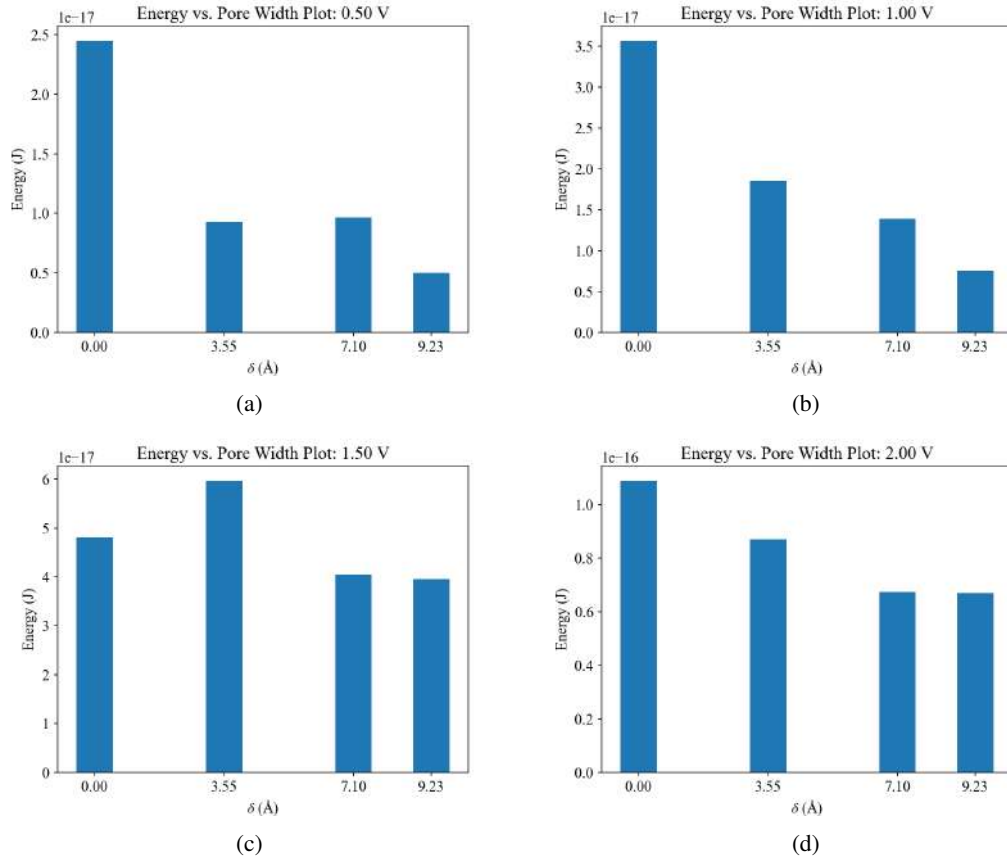
Figure 4.15: Electrical energy stored for each capacitor at potential drop values (a) 0.50 V, (b) 1.00 V, (c) 1.50 V, and (d) 2.00 V.

This shows that the most energy stored was within the planar model. This is because the charge values for the capacitors with nano-slit pore electrodes is lower. This calculation affects the nano-slit pore model with $\delta = 3.55$ Å because its had the highest capacitance value with a lower charge value than the planar model, resulting in a lower energy value calculated almost consistently against the planar model.

Chapter 5

Conclusions and Recommendations

5.1 Conclusions

The attempt to simulate EES using a graphene-TiO$_2$ electrode supercapacitor was successful, with simulations running for 100000 timesteps for both models. However, the measurements for the charges and capacitance have proven to be inaccurate compared to literature, which may be attributed to the package still being new [24]. That aside, the supercapacitor model used in this study exhibited capacitive properties nonetheless. The nano-slit pore model electrode with $\delta = 3.55$ Å showed both the highest capacitance and surface capacitance values.

5.2 Recommendations

The following recommendations are suggested for future researchers.

First, it is suggested for future studies to attempt the usage of an *ab initio* MD simulator. This model of MD may provide additional insight that classical dynamics simulators may not be capable of modelling yet. Furthermore, any deviations between the result of such study in the future and this one must be taken into consideration.

Second, considering the results of this study, it is recommended that an experimental study be conducted, similar to that in reference [21]. One may incorporate changes to that study using the findings of this one, which are the following. First, the usage of a TiO$_2$ as a layer separating the graphene electrodes and the electrolyte. Second, the incorporation of slit pores into an actual electrode has shown in this study to improve the capacitance for specific pore widths.

Finally, should more studies use LAMMPS as a method of simulation for EES, it is recommended to change different parameters of the study. The electrolyte used, the concentration of the electrolyte, the size of the simulation box, and the timestep length used for running the simulations is recommended. It is suggested that a powerful desktop computer be used for this, however, since experiences with using laptops have led to prolonged simulations.

Literature Cited

[1] R. A. Freedman, H. D. Young, and A. L. Ford, *University Physics with Modern Physics, 13th ed.* Addison-Wesley, 2012, ch. 24: Capacitance and Dielectrics.

[2] O. Haas and E. J. Cairns, "Electrochemical energy storage," *Annual Reports Section "C" (Physical Chemistry)*, vol. 95, no. 6, pp. 163 – 198, 1999.

[3] S. Sagadevan, A. R. Marlinda, Z. Z. Chowdhury, Y. B. A. Wahab, N. A. Hamizi, M. M. Shahid, F. Mohammad, J. Podder, and M. R. Johan, "Fundamental electrochemical energy storage systems," *Advances in Supercapacitor and Supercapattery*, 2021.

[4] P. L. Antonucci and V. Antonucci, *Energy Storage in the Emerging Era of Smart Grids*. InTech, 2011, ch. 1: Electrochemical Energy Storage.

[5] T. P. Sumangala, M. S. Sreekanth, and A. Rahaman, *Handbook of Nanocomposite Super-capacitor Materials III.* Springer, 2021, ch. 11: Applications of Supercapacitors.

[6] S. A. Hollingsworth and R. O. Dror, "Molecular dynamics simulation for all," *Neuron*, vol. 99, no. 6, pp. 1129–1143, 2018.

[7] J. Niskanen and H. Henschel, "Molecular dynamics simulations: Lecture 1," 2013.

[8] LAMMPS Developers, "LAMMPS Molecular Dynamics Simulator." [Online]. Available: https://www.lammps.org/#gsc.tab=0

[9] Theoretical and Computational Biophysics GroupUniversity of Illinois at Urbana-Champaign and National Institute of Health, "What is VMD?" [Online]. Available: https://www.ks.uiuc.edu/Research/vmd/allversions/what_is_vmd.html

[10] OVITO, "About OVITO." [Online]. Available: https://www.ovito.org/about/

[11] J. Libich, J. Máca, J. Vondrák, O. Čech, and M. Sedlaříková, "Supercapacitors: Properties and applications," *Journal of Energy Storage*, vol. 17, 2018.

[12] M. Chen, Y. Zhang, G. Xing, S. L. Chou, and Y. Tang, "Electrochemical energy storage devices working in extreme conditions," *Energy & Environmental Science*, 2021.

[13] X. Wang, M. Salari, D. E. Jiang, J. C. Varela, B. Anasori, D. J. Wesolowski, S. Dai, M. W. Grinstaff, and Y. Gogotsi, "Electrode material–ionic liquid coupling for electrochemical energy storage," *Nature Review Materials*, vol. 5, pp. 787–808, 2020.

[14] Philippine Department of Energy, "National renewable energy program." [Online]. Available: https://www.doe.gov.ph/national-renewable-energy-program?withshield=1

[15] M. D. Stoller, S. Park, Y. Zhu, J. An, and R. S. Ruoff, "Graphene-based ultracapacitors," *Nano Letters*, vol. 8, 2008.

[16] T. P. Sumangala, M. S. Sreekanth, and A. Rahaman, *Handbook of Nanocomposite Super-capacitor Materials III*. Springer, 2021, ch. 5: Electrode Material Selection for Superca-pacitors.

[17] L. L. Zhang, R. Zhou, and X. S. Zhao, "Graphene-based materials as supercapacitor elec-trodes," *Journal of Materials Chemistry*, 2010.

[18] J. R. Lake, A. Cheng, S. Selverston, Z. Tanaka, J. Koehne, M. Meyyappan, and B. Chen, "Graphene metal oxide composite supercapacitor electrodes," *Journal of Vacuum Science and Technology B*, 2012.

[19] R. Liang, Y. Du, P. Xiao, J. Cheng, S. Yuan, Y. Chen, J. Yuan, and J. Chen, "Transition metal oxide electrode materials for supercapacitors: A review of recent developments," *Nanomaterials (Basel)*, vol. 11, no. 5, 2021.

[20] C. Xiang, M. Li, M. Zhi, A. Manivannanc, and N. Wu, "Reduced graphene oxide/titanium dioxide composites for supercapacitor electrodes: shape and coupling effects," *Journal of Materials Chemistry*, vol. 22, 2012.

[21] A. Ramadoss and S. J. Kim, "Improved activity of a graphene-TiO_2 hybrid electrode in an electrochemical supercapacitor," *Carbon*, vol. 63, 2013.

[22] D. Marrocchelli, C. Merlet, and M. Salanne, "Molecular dynamics simulations of elec-trochemical energy storage devices," *Physical Multiscale Modeling and Numerical Sim-ulation of Electrochemical Devices for Energy Conversion and Storage: From Theory to Engineering to Practice*, pp. 61–89, 2016.

[23] A. P. Thompson, H. M. Aktulga, R. Berger, D. S. Bolintineanu, W. M. Brown, P. S. Crozier, P. J. in 't Veld, A. Kohlmeyer, S. G. Moore, T. D. Nguyen, R. Shan, M. J. Stevens, J. Tranchida, C. Trott, and S. J. Plimpton, "LAMMPS - a flexible simulation tool for particle-based materials modeling at the atomic, meso, and continuum scales," *Computer Physics Communications*, vol. 271, 2022.

[24] L. J. V. Ahrens-Iwers, M. Janssen, S. R. Tee, and R. H. Meißner, "ELECTRODE: An electrochemistry package for atomistic simulations," *Journal of Chemical Physics*, vol. 157, 2022.

[25] G. F. L. Pereira, E. E. Fileti, and L. J. A. Siqueira, "Comparing graphite and graphene oxide supercapacitors with a constant potential model," *Journal of Physical Chemistry C*, vol. 25, pp. 2318–2326, 2021.

[26] M. Galib, M. M. Hosen, J. K. Saha, M. M. Islam, S. H. Firoz, and M. A. Rahman, "Electrode surface modification of graphene-MnO_2 supercapacitors using molecular dynamics simulations," *Journal of Molecular Modeling*, vol. 26, 2020.

[27] A. Szewczyk, J. Sikula, V. Sedlakova, J. Majzner, P. Sedlak, and T. Kuparowitz, "Voltage dependence of supercapacitor capacitance," *Metrology and Measurement Systems*, vol. 23, 2016.

[28] S. Gravelle, "Nanosheared electrolyte." [Online]. Available: https://lammpstutorials. github.io/sphinx/build/html/tutorials/level2/nanosheared-electrolyte.html?fbclid= IwAR39viFCMrazMNIoNNflppSdLEUygQ86ndn_d1T2WBGipBYK3t-7XDxVzyg

[29] LAMMPS Developers, "lattice command." [Online]. Available: https://docs.lammps.org/ lattice.html

[30] LAMMPS Developers, "region command." [Online]. Available: https://docs.lammps.org/ region.html

[31] LAMMPS Developers, "create_box command." [Online]. Available: https://docs.lammps. org/create_box.html

[32] LAMMPS Developers, "create_atoms command." [Online]. Available: https://docs. lammps.org/create_atoms.html

[33] Materials Project, "TiO$_2$." [Online]. Available: https://next-gen.materialsproject. org/materials/mp-2657#:\sim:text=TiO%E2%82%82%20is%20Rutile%20structured% 20and,)%20Ti%E2%80%93O%20bond%20lengths.

[34] LAMMPS Developers, "molecule command." [Online]. Available: https://docs.lammps. org/molecule.html

[35] LAMMPS Developers, "fix command." [Online]. Available: https://docs.lammps.org/fix. html

[36] LAMMPS Developers, "run command." [Online]. Available: https://docs.lammps.org/ run.html

[37] LAMMPS Developers, "set command." [Online]. Available: https://docs.lammps.org/set. html

[38] LAMMPS Developers, "write_data command." [Online]. Available: https://docs.lammps. org/write_data.html

[39] LAMMPS Developers, "write_dump command." [Online]. Available: https://docs. lammps.org/write_dump.html

[40] LAMMPS Developers, "group command." [Online]. Available: https://docs.lammps.org/ group.html

[41] LAMMPS Developers, "dump command." [Online]. Available: https://docs.lammps.org/ dump.html

[42] University of Oregon Macromolecular Crystallography, "Molecular Dynamics - Statistical Ensembles." [Online]. Available: https://www.uoxray.uoregon.edu/local/manuals/biosym/ discovery/General/Dynamics/Ensembles.html#NVE

[43] LAMMPS Developers, "fix nve/limit command." [Online]. Available: https://docs. lammps.org/fix_nve_limit.html

[44] LAMMPS Developers, "fix shake command." [Online]. Available: https://docs.lammps. org/fix_shake.html

[45] LAMMPS Developers, "fix recenter command." [Online]. Available: https://docs.lammps. org/fix_recenter.html

[46] LAMMPS Developers, "timestep command." [Online]. Available: https://docs.lammps. org/timestep.html

[47] LAMMPS Developers, "thermo command." [Online]. Available: https://docs.lammps.org/ thermo.html

[48] LAMMPS Developers, "boundary command." [Online]. Available: https://docs.lammps. org/boundary.html

[49] LAMMPS Developers, "include command." [Online]. Available: https://docs.lammps. org/include.html

[50] LAMMPS Developers, "kspace_modify command." [Online]. Available: https://docs. lammps.org/kspace_modify.html

[51] LAMMPS Developers, "fix electrode/conp command." [Online]. Available: https: //docs.lammps.org/fix_electrode.html

[52] LAMMPS Developers, "thermo_style." [Online]. Available: https://docs.lammps.org/ thermo_style.html

[53] LAMMPS Developers, "fix nvt command." [Online]. Available: https://docs.lammps.org/ fix_nh.html

[54] LAMMPS Developers, "variable command." [Online]. Available: https://docs.lammps. org/variable.html

[55] LAMMPS Developers, "compute command." [Online]. Available: https://docs.lammps. org/compute.html

[56] C. Merlet, M. Salanne, B. Rotenberg, and P. A. Madden, "Imidazolium ionic liquid interfaces with vapor and graphite: Interfacial tension and capacitance from coarse-grained molecular simulations," *Journal of Physical Chemistry*, 2011.

[57] N. Michaud-Agrawal, E. J. Denning, C. Beckstein, J. L. Adelman, S. Agarwal, I. Alibay, A. Angaria, L. P. B. Araújo, Balasubramanian, U. Bansal, J. Barnoud, T. Bengtsen,

A. Bernardin, N. Bhat, M. Bieniek, W. Boomsma, J. Borreguero, C. Bouysset, B. Bruininks, S. Buchoux, S. von Bülow, D. Caplan, Y. Chang, M. Chavent, H. Chen, K. Clark, C. Cook, R. Cortini, N. Craven, R. Crehuet, D. Cruz, R. Delgado, J. Detlefs, X. Deupi, J. Domanski, D. L. Dotson, A. Ehlen, S. Fan, L. van der Feltz, P. Fowler, G. Fraux, W. Glass, J. Goose, R. J. Gowers, L. Grossar, A. Gupta, A. Gupta, B. Hall, A. Harmalkar, I. Hristov, E. Hruska, K. J. Huston, S. Jain, J. Jordan, J. Kapla, N. Khare, A. W. King, A. A. Kognole, M. Linke, P. Loche, J. Lu, H. MacDermott-Opeskin, M. Matta, A. R. McCluskey, R. McGibbon, R. Meli, M. N. Melo, D. R. Mierzejewski, H. Mull, M. L. Nance, F. B. Naughton, A. Nesterenko, H. Nguyen, S. Y. Noh, D. Padula, N. Pal, M. F. Palermo, D. Parton, S. Pathak, J. L. Phillips, K. Punjani, M. Quevillon, V. Rathore, T. Reddy, P. Reis, P. Rigor, A. Rizzi, C. Y. S, U. Saxena, M. Sega, S. L. Seyler, F. Shah, A. Shandilya, S. Sharma, P. Smith, A. Somogyi, C. S. Souza, S. Srivastava, L. Stelzl, G. Stock, F. Suchak, A. Suhane, M. Tadema, J. M. C. Teixeira, X. Tempula, M. W. Thompson, H. Tian, M. Tiberti, W. van der Toorn, I. Virshup, L. Wang, N. Wendt, Z. Wu, Z. Xue, J. E. Zamora, J. Zeman, Y. Zhang, Y. Zhuang, , and O. Beckstein, "15. constants and unit conversion −." [Online]. Available: https://docs.mdanalysis.org/1.1.0/documentation_pages/units.html

Appendix A

Content of the Parameters File (PARM.lammps)

```
#PARM file specifications for the atoms in the system


mass 1 15.9994 # oxygen water

mass 2 1.008 # hydrogen water

mass 3 1.008 # hydrogen water

mass 4 22.9898 # sodium

mass 5 35.453 # chlorine

mass 6 12.011 # carbon top

mass 7 47.867 # titanium top

mass 8 15.9994 # oxygen (tio2) top

mass 9 12.011 # carbon top

mass 10 47.867 # titanium top

mass 11 15.9994 # oxygen (tio2) top


pair_coeff 1 1 0.185199 3.1589 # oxygen water

pair_coeff 2 2 0.0 0.0 # hydrogen water

pair_coeff 3 3 0.0 0.0 # hydrogen water

pair_coeff 4 4 0.1144 3.38 # sodium

pair_coeff 5 5 0.1144 3.38 # chlorine

pair_coeff 6 6 0.12000000 3.29630000 # carbon top

pair_coeff 7 7 0.2200 2.4244 # titanium top

pair_coeff 8 8 0.324 1.2958 # oxygen (tio2) top

pair_coeff 9 9 0.12000000 3.29630000 # carbon bot

pair_coeff 10 10 0.2200 2.4244 # titanium bot

pair_coeff 11 11 0.324 1.2958 # oxygen (tio2) bot


bond_coeff 1 0 0.9572 # water
```

```
angle_coeff 1 0 104.52 # water
```

Appendix B

Expression conditions for the nano-slit pore models in OVITO

B.1   For 3.55-Å nano-slit pore

```
(Position.X <= 17.2736 && Position.X >= 13.7236) && (ParticleType == 5
|| ParticleType == 6 || ParticleType == 7 || ParticleType == 8 ||
ParticleType == 9 || ParticleType == 10)
```

B.2   For 7.10-Å nano-slit pore

```
(Position.X >= 11.9487 && Position.X <= 19.0486) && (ParticleType == 5
|| ParticleType == 6 || ParticleType == 7 || ParticleType == 8 ||
ParticleType == 9 || ParticleType == 10)
```

B.3   For 9.23-Å nano-slit pore

```
(Position.X <= 20.1136 && Position.X >= 10.8836) && (ParticleType == 5
|| ParticleType == 6 || ParticleType == 7 || ParticleType == 8 ||
ParticleType == 9 || ParticleType == 10)
```

Appendix C

Constant Potential Simulation Code

```
# electrodes with constant potential
# for graphene-ionic liquid supercapacitor


boundary p p f # slab calculation
include settingsplanar.mod # styles, groups, computes and fixes
kspace_modify slab 3.0


fix conp ebot electrode/conp -0.25 1.979 couple etop 0.25 symm on


dump 1 all custom 50 conp_run.lammpstrj id type xs ys zs vx vy vz fx fy fz


thermo 50
thermo_style custom step temp c_ctemp1 epair etotal c_qbot c_qtop
write_data conp_planar.data
run 100000


# 0.5 V potential drop
```